Natural Resources Canada Ressources naturelles Canada

GEOLOGICAL SURVEY OF CANADA
OPEN FILE 8824

Multispectral permafrost terrain classification, Rankin Inlet, Nunavut

G.A. Oldenborger, B. Faucher, and A.-M. LeBlanc

2021

Canada

GEOLOGICAL SURVEY OF CANADA
OPEN FILE 8824

Multispectral permafrost terrain classification, Rankin Inlet, Nunavut

G.A. Oldenborger[1], B. Faucher[2], and A.-M. LeBlanc[1]

[1]Geological Survey of Canada, 601 Booth Street, Ottawa, Ontario
[2]Department of Geography, Environment and Geomatics, University of Ottawa, 60 University Private, Ottawa, Ontario

2021

Permanent link: https://doi.org/10.4095/328869

This publication is available for free download through GEOSCAN (https://geoscan.nrcan.gc.ca/).

Recommended citation
Oldenborger, G.A., Faucher, B., and LeBlanc, A.-M., 2021. Multispectral permafrost terrain classification, Rankin Inlet, Nunavut; Geological Survey of Canada, Open File 8824, 38 p. https://doi.org/10.4095/328869

Publications in this series have not been edited; they are released as submitted by the author.

SUMMARY

This Open File reports on permafrost terrain classification using multispectral WorldView-2 satellite imagery over Rankin Inlet, Nunavut. A suite of images was processed to yield a single corrected multispectral mosaic image for a 1360 km^2 area inland of the Hamlet of Rankin Inlet where permafrost studies are ongoing. Terrain classes relevant to permafrost conditions and thaw sensitivity were defined using existing on-the-ground knowledge of vegetation, surficial geology, hydrology, ground temperature, and ground ice occurrence for the region. At locations for two separate study sites (15 km^2 and 7 km^2), a number of reference areas were established and classified using visual interpretation of the imagery in combination with ground truth information from the sites. Given the reference classifications, permafrost terrain mapping was performed using maximum likelihood classification of the multispectral data alone (MS), and in conjunction with the derivative measure of texture (T), and the independent variable of topography transformed to topographic position index (TPI). Classification performance was assessed using true positive rate (TPR) and positive predictive value (PPV), along with detailed analysis of the confusion matrix. Classification results were validated by visual examination of the class maps and imagery, and by qualitative comparison to surficial geology. The full MS+T+TPI feature set provides the best overall classification with prediction accuracy for the reference areas of approximately 85% (TPR and PPV) for both study sites. However, significant misclassification persists as indicated by the full confusion matrix. In some cases, misclassification occurs between classes with similar spectral and topographic characteristics, but also similar permafrost conditions, such that misclassification is of limited consequence. In other cases, misclassification occurs between classes with similar spectral and topographic characteristics, but distinct thaw sensitivity, and the potential for misclassification must be carefully considered.

TABLE OF CONTENTS

INTRODUCTION

Permafrost conditions can exhibit heterogeneity and variability over the landscape in response to variations in surficial geology, availability of water, vegetation, and other factors (French and Shur, 2010; O'Neil et al., 2019). Information on permafrost conditions is important for predicting the response of the landscape to warming, and its sustainability as an engineering substrate in terms of thaw subsidence. However, the scarcity of permafrost data may prevent the characterization of permafrost and thermophysical conditions at a regional scale (Smith et al., 2010). Remote sensing data can be used to extend on-the-ground knowledge, provided that a relationship can be established between the remotely sensed data and permafrost conditions. Multispectral satellite images provide a band-limited representation of the spectral reflectance of the land surface that contains information on the constituent materials and land cover (Lillesand et al., 2015). Many of the same factors that influence spectral reflectance, such as material type, vegetation and soil moisture also influence permafrost. As such, there may exist some relationship to be learned between multispectral data and permafrost conditions. This report explores the potential for permafrost terrain mapping via supervised classification of multispectral satellite imagery and supporting data in the vicinity of Rankin Inlet, Nunavut.

Permafrost terrain mapping is analogous to land cover mapping of bio-physical conditions (e.g., Olthof et al., 2009), or remote predictive mapping of surficial geology (e.g., Grunsky et al., 2006; LaRocque et al., 2012; Campbell et al., 2013) or bedrock (e.g., Behnia et al., 2012). Permafrost terrain mapping is distinctive in that the target terrain units for classification are defined in terms of relevance specifically to permafrost conditions, and may not reflect a particular vegetative regime, or surficial material. Rather, permafrost terrain units or classes are defined according to combinations of surficial geology, vegetation, surface water, geomorpholgy, permafrost landforms, and other landscape features that are known to significantly influence or be indicative of ground ice conditions or thaw sensitivity. The permafrost terrain classifications generated from multispectral imagery are intended to be informative for inferring permafrost degradation potential, but are not definitive, and should be considered a complement to other sources of information in permafrost studies.

STUDY AREA

The Hamlet of Rankin Inlet is located on the western coast of Hudson Bay in the Kivalliq Region of Nunavut, Canada (Figure 1). The region was covered by the Laurentide Ice Sheet during the Wisconsin Glaciation (Dyke, 2004). After deglaciation, the postglacial Tyrrell Sea extended inland over the isostatically depressed land surface. Post-glacial isostatic rebound and emergence resulted in the formation of subaerial permafrost that continues to evolve.

The surficial geology consists of glacial, glaciofluvial, marine, alluvial, and organic deposits over bedrock (McMartin, 2002). The glacial deposits are unsorted to poorly sorted tills with a silty sand matrix. The postglacial sea resulted in deposition of marine, nearshore, and beach sediments along with reworking of glacial sediments. In many locations, wave washing resulted in isolation of coarse till components and accumulation of fine silt and sand at lower elevations as nearshore marine deposits. The topography consists of undulating bedrock hills, eskers, moraines, and drumlins with a network of rivers draining the area toward Hudson Bay. Small lakes are abundant and located in depressions related to bedrock basins and glacial landforms. Most of the study area is covered with tundra vegetation typical of the low-arctic region (mosses, herbaceous plants, shrubs, and alpine-arctic plants).

Rankin inlet is within the continuous permafrost zone where 90% to 100% of the land area is underlain by permafrost (Heginbottom et al., 1995) with the potential for low to medium segregated ice abundance (O'Neill et al., 2019). Periglacial landforms such as ice-wedge polygons, mud boils, gelifluction lobes, and active layer detachments are abundant (McMartin, 2002). Mean annual ground temperature at the top of permafrost varies from −9.5 to −5.5°C and active layer thickness ranges from 60 to 160 cm (LeBlanc and Oldenborger, 2021). Surface conditions including surficial geology, soil moisture, drainage and snow cover are identified as major factors contributing to variations in thermophysical conditions. An ice-rich active layer and ice-rich top of permafrost are identified (but not everywhere or exclusively) in alluvial and marine sediments, and in nearshore marine sediments. Presence of a thick active layer and ice-poor top of permafrost in marine and nearshore marine sediments is attributed to high thermal conductivity resulting from soil moisture and/or flooding (LeBlanc and Oldenborger, 2021).

METHODS

Multispectral Satellite Images

WorldView-2 imagery is an optical satellite imagery product commercially available from DigitalGlobe (now Maxar Technologies) consisting of images of spectral reflectance in eight bands. Native ground sample distance (GSD) at nadir is 0.46 m for panchromatic data and 1.85 m for multispectral data with 11-bit digitization. Imagery was acquired over a 40 km × 34 km area inland of Rankin Inlet for the date of July 22, 2017 (Figure 1). Data were acquired from MDA Geospatial Services as 35 tiles of Standard Ortho Ready (Level 2A) 8-bit imagery in three panels at 0.5 m GSD for panchromatic data, and 2 m GSD for four multispectral bands: Blue (450–510 nm), Green (510–580 nm), Red (630–690 nm), and Near Infrared (770–895 nm). The imagery was commercially corrected for radiometric distortion, sensor geometry, and optical distortion to give at-sensor radiance for a vertical image.

Image panels were imported to *PCI Geomatica* and atmospheric corrections were calculated and applied using the *ATCOR Ground Reflectance* module, which also applies a transformation of image radiance to top-of-atmosphere reflectance. Sensor parameters and satellite viewing geometry were acquired from the panel metadata. No clouds were visible in the images, but haze removal was performed with 50% coverage. Aerosol types and conditions were set as *rural* and *subarctic summer* for atmospheric information.

Following atmospheric correction, the image panels were individually orthorectified using the *OrthoEngine* module and the Natural Resource Canada High-Resolution Digital Elevation Model (HDREM) that incorporates data from the ArcticDEM (Morin et al., 2016; http://arcticdem.org). Mapping parameters were set as *optical satellite modelling* and *rational function (extract from image)*, with the final projection being WGS84 UTM 15N at native GSD. Image panels were subsequently assembled into a single mosaic preserving the four spectral bands using the *Mosaic* tool. Mosaic normalization was performed with an adaptive filter at 20%. Colour balancing of the mosaic (global adjustment of the image spectra to minimize differences between overlapping areas) was performed using the bundle method. In a final step, the panchromatic data were used with the *MRAFUSION* algorithm for pansharpening the multispectral data to produce an atmospherically corrected and normalized 1360 km^2 4-band mosaic raster of the study area projected with a pansharpened GSD of 0.5 m (Figure 2).

Reference Classification

Within the multispectral mosaic, two separate study sites were selected for which on-the-ground permafrost information has been gathered (RI05, RI08; Figure 2). Permafrost information for these sites includes ground temperatures and ground ice conditions (Oldenborger et al., 2017; LeBlanc and Oldenborger, 2021), surficial geology and landforms (McMartin, 2002), and ground subsidence with associated thaw sensitivity (LeBlanc et al., 2019; Oldenborger et al. 2020). Existing knowledge of permafrost conditions, observations of vegetation, and observations of hydrology were combined with detailed visual interpretation of the imagery to define and classify reference areas with distinct permafrost conditions and/or thaw sensitivity for the study sites. Hung et al. (2020) report that pansharpening does not significantly improve land cover classification accuracy. However, pansharpening is not detrimental to the classification, and it was found to be beneficial for reference classification.

The permafrost terrain reference classification is summarized in Table 1 where the class descriptions detail the types of landforms, vegetation and surficial geology intentionally included within that class. The classes are common to both study sites, although bedrock (Class 12) is not present at Site RI05 (GSC, 2017). The reference classifications account for approximately 3.9% and 6.6% of the areas of the RI05 and RI08 sites, respectively (Figure 3). On-the-ground photographic examples of a selection of the reference classes are shown in Figure 4. The reference classifications are the result of several iterations of independent interpretation between multiple interpreters, but no further consideration is given to errors associated with the reference classifications, and they are implicitly assumed to have negligible error (e.g., Foody, 2002). The reference classifications were neither targeted to any specific areas, nor distributed by any random sampling scheme, but rather are subjective in distribution (both spatially and proportionally between classes) and represent characteristic examples of the defined classes. The reference classification is imbalanced and may or may not contain sampling bias, which occurs when there is a difference in class distribution between the reference and the population.

Texture

Classifying terrain using the 4-band WorldView-2 mosaic is a form of spectral pattern recognition, in that each pixel is classified based on the properties of that single pixel (e.g., Lillesand et al., 2015). Spectral pattern recognition is subject to spectral overlap, wherein individual classes do not always exhibit unique or separable spectral signatures. To increase the potential separability between permafrost terrain classes beyond that capable from the multispectral data alone, texture can be introduced as an additional image feature. Texture may be defined as the combination of the magnitude and frequency of tonal change in an image, where tone refers to the magnitude of the image variable (Drury, 1993). Arrangements of similar textures result in patterns that can be used in image interpretation and segmentation. Adding texture to the analysis is a way of incorporating spatial information, or information on pixel neighbours, such that the classification involves both spectral and spatial pattern recognition, without the need to define spatially demarcated objects.

Texture can be added as an image feature (or set of features) using a variety of methods ranging from complicated wavelet scattering (Andén and Mallat, 2014), to space-local frequency analysis (Oldenborger et al., 2002), to measures of variability such as standard deviation, range, or gradient (Humeau-Heurtier, 2019). The key element is that texture is a spatial quantity and its realization must involve some neighbourhood of pixels. Edge density is a measure of texture that is easy to implement with linear filters in a GIS environment, and is useful when little is known about orientation of texture (e.g., Williams et al., 1998). Edge detection is applied to the panchromatic image for each site using a 4-pixel derivative search radius and a 9-pixel Gaussian pre-smoothing filter with 4-pixel variance. Neighbourhoods with abundant tonal variation are characterized by the presence of many edges. As such, texture is calculated as edges per area using a moving average window. Using this method, texture is scale dependent and the averaging window size should be chosen to be large enough to capture many of the image objects that define the texture, but small enough that it is contained within areas of similar texture. Trial and error was used to arrive at a

70×70 m^2 window that captures textural objects such as mudboils and hummocks, yet falls within individual terrain units.

Residual Elevation

While texture is a derivative feature of the multispectral data, topography provides an independent feature that may improve separability in classification of remote sensing data (e.g., LaRocque et al., 2012). Guisan et al. (1999) introduced the Topographic Position Index (TPI) to represent the residual elevation as a predictor variable for classification of tree and shrub species based on the assertion that topographic position is correlated with ecological variables that influence vegetation. Similarly, topographic position is expected to be correlated with ecological variables that influence permafrost conditions and thaw sensitivity, such as vegetation itself, but also soil moisture and snow depth.

In contrast to absolute elevation, but similar to texture, TPI is dependent on a neighbourhood of pixels and is scale-dependent. Use of TPI can ameliorate elevation bias that might otherwise be associated with the reference classification. Using the HRDEM, TPI was calculated using the difference from the mean of a 1×1 km^2 moving average window. At this scale, the TPI represents the medium-scale topographic hierarchy of hill tops and valley bottoms for the study area. Window sizes much smaller than 1 km result in TPI distributions that are indicative of breaks in slope. In contrast, larger window sizes result in a regionally levelled measure of topography. Additional trials were performed with Topographic Wetness Index (TWI) as an independent feature, but TWI exhibited micro-scale drainage features that resulted in misclassification.

Classification

The features of the four multispectral bands, texture and TPI for each study site are shown in Figures 5 and 6. Permafrost terrain classification was performed using maximum likelihood classification (MLC) within *PCI Geomatica*. MLC is a form of machine learning that determines the most probable membership of a particular datum (pixel) to one of a set of observed classes given by the reference classification (e.g., Lillesand et al., 2015). In general, the following conditions should hold for application of MLC: 1) the features should exhibit stationary normal distributions, and 2) features should not exhibit strong correlation (e.g., Hogland et al., 2013). He et al., (2015) demonstrate that MLC is relatively robust with respect to deviations from a multi-variate normal distribution. For the Rankin Inlet data, nearly all of the reference classes (Table 1) exhibit approximately normal distributions with the exception of deep water (Class 1) that exhibits a slightly bi-modal distribution of multispectral data. Furthermore, although correlation exists between the blue, green, and red bands of the WorldView-2 mosaic, it is not sufficient to render the covariance matrix not positive definite.

MLC was performed separately for each study site in four stages or four different feature sets: 1) initial classification of the multispectral data alone (MS), 2) classification with texture (MS+T), 3) classification with residual elevation (MS+TPI), and 4) classification with texture and residual elevation (MS+T+TPI). For each stage, classification results were assessed using statistical performance indicators and visual inspection of the classification involving comparison against on-the-ground observations and surficial geology. Classification accuracy is measured in terms of the resubstitution error, or classification of the reference areas (e.g., Lillesand et al., 2015). Although this method only measures classification performance in the same areas used to train the model (which are typically good examples of defined classes), it allows all of the reference data to be used for training. Being an over-determined, low-complexity parametric model (with no hyperparameters), MLC is not subject to errors associated with imbalanced data, or with over-fitting or memorization of the reference data. It is subject to differences in the data distribution between the reference set and the general population. The resubstitution accuracy is expected to be at least as good, but likely better than generalized accuracy, such that the reported accuracy is an over-estimate of the true classification performance (e.g., Hammond and Verbyla, 1996).

The confusion matrix provides the information for the analysis of statistical classification performance (e.g, Foody, 2002). The diagonal of the confusion matrix provides the True Positive Rate (TPR), or producer's accuracy of classification for each class. However, TPR does not account for occurrence of false positives or class prevalence. Instead, the Positive Predictive Value (PPV), or user's accuracy of classification provides a combined measure of the number of true and false positives mapped. Additionally, the confusion matrix can be weighted by class prevalence over the entire classification to yield population proportional area that better represents the entire mapped region (Stehman and Foody, 2019). In the case of well-predicted but non-prevalent classes, such a transformation typically results in decreased TPR (the PPV does not change). Class-averaged TPR and PPV provide some indication of performance for the entire classification, but may not reflect strongly disparate class-based accuracy.

Furthermore, while class-based TPR and PPV provide measures of performance, understanding the uncertainty associated with the classification requires more detailed examination of the confusion matrix. To summarize the details of the confusion matrix, a "confusion descriptor" is introduced comprised of two parts for each class. The first part of the confusion descriptor indicates what other classes are likely to be predicted or mapped for a class in the reference classification (the producer's view) and the second part of the confusion descriptor indicates what classes in the reference classification are likely to be present when a class is predicted (the user's view). An example confusion descriptor for Class x is "sometimes mapped as Class z; often confused with Class y, rarely confused with Class z" where the ratio r of false negatives (or false positives) to true positives for Class x is used to define the terms *often*: $r >= 0.5$, *sometimes*: $0.5 > r >= 0.05$, and *rarely*: $0.05 >= r > 0.005$. Confusion descriptors are based on population proportional area to better represent the entire classification as opposed to only the reference set. Similar descriptors are obtained using pixel counts with differences associated with highly variable prevalence, but the same descriptors cannot be obtained from a confusion matrix normalized to proportions relative to the reference class.

RESULTS

Class maps for the four feature sets at each study site are shown in Figures 7 and 8. The predicted area of each class for the different feature sets is illustrated in Figure 9 for both study sites. Classification performance (TPR and PPV) for the different feature sets is summarized in Tables 2 and 3 for study sites RI05 and RI08, respectively. The full confusion matrices for each stage, prevalence, and population proportional area are given in Appendices A and B for study sites RI05 and RI08, respectively.

If only the performance metrics are considered, it is apparent that the MS-only classification is the worst performer for both study sites, with high accuracy for a few classes, but low accuracy for others. The addition of texture and TPI individually both serve to improve classification accuracy for nearly all classes at both study sites. Texture and TPI combined increases accuracy even further and reduces the discrepancy of accuracy between classes. The addition of texture is the most influential on the classification of dry patterned ground (Class 9) and wet vegetation (Class 11), both of which are characterized by particular patterns of tonal variation: mud boils and hummocks, respectively (Table 1). In particular, texture reduces the occurrence of dry patterned ground (Class 9) being incorrectly classified as dry polygonal ground (Class 7), and wet vegetation (Class 11) being incorrectly classified as flooded vegetation (Class 5) or wet polygonal ground (Class 8) as evidenced by the changes in the confusion matrices (Appendices A and B).

In contrast, TPI exhibits significant influence on classes that occupy particular spots in the topographical hierarchy, such as raised beaches and eskers that dominate the high ground, and polygonal ground which is typically found in low-lying valleys. In particular, TPI reduces the occurrence of beaches (Class 6) being misclassified as wet polygonal ground (Class 8) or wet vegetation (Class 11) which are other dark terrain types, although there are differences in improvement between the study sites (Appendices A and B). TPI also greatly reduces the occurrence of dry polygonal ground (Class 7) being misclassified as till plain (Class 10) which are both green terrain types, but have significantly different permafrost conditions. For both sites, only the MS+T+TPI feature set achieves an average accuracy greater than 85% for both TPR and PPV, although there are still some classes of lower accuracy. While a more rigorous accuracy threshold could be established for a particular end user that might justify acceptance of a different feature set, it is clear that the MS+T+TPI feature set provides the highest classification accuracy.

However, accuracy measures alone do not necessarily indicate the best feature set for classification. Results must also be evaluated in the context of existing knowledge. The maps in Figures 7 and 8 show that when using only multispectral features, the classifications are extremely variable and heterogeneous despite having similar predicted class areas (Figure 9). The spectral closeness and overlap of reference classes result in juxtapositions of mapped classes that are physically unrealistic, such as wet polygonal ground (Class 8) surrounded by raised beach (Class 6) on topographic highs. Both texture and TPI act to consolidate the classifications into more continuous units with more geologically realistic adjacencies. However, this is not without a trade-off. As shown in Figure 9, texture acts to introduce a large amount of dry patterned ground (Class 9) at the expense of till and wet vegetation (Classes 10 and 11) which are expected to be more prevalent (McMartin, 2002). TPI alone is more stable, but can introduce a strong topographic imprint and misclassifications due to topography, such as over-prediction of dry and wet polygonal ground (Classes 7 and 8) particularly along lake shores (Figure 7). TPI can also result in misclassification if the reference classification is not representative of all topographic positions for a particular class. The problems of texture and TPI alone are somewhat ameliorated by their joint application.

Comparison to Surficial Geology

The permafrost terrain classifications can also be evaluated in terms of the surficial geology mapped for the region (GSC, 2017). Although the reference classification is based on permafrost terrain types, there is a correspondence to surficial geology (Table 1) that can be used for validation of the classifications. However, since the correspondence is neither unique nor one-to-one, validation using surficial geology should be considered as qualitative and not conclusive.

The distribution of surficial geology over each permafrost terrain class is shown in Figure 10 for Sites RI05 and RI08 combined using the MS+T+TPI feature set. Areas classified as exposed sand and gravel (Class 3) correspond largely to sand and gravel beach (Mr) and esker (GFc) deposits as expected, but also to undifferentiated till and marine (T.M) sediments that should not yield exposed sand and gravel when eroded. Closer inspection of the mosaic reveals that areas classified as exposed sand and gravel (Class 3), but mapped as T.M, are actually littoral sediments without vegetation. In this case, the classification provides a means of refining geological maps that may be produced using lower resolution information, or by merging and standardization of different data sources.

Areas classified as dry water body and wet vegetation (Classes 4 and 5) correspond in order of prevalence to undifferentiated till and marine (T.M), nearshore marine (Mn), and alluvial (A and A.M) sediments, which is understandable in terms of modern lakes and streams on till plains and valley bottoms. Areas classified as beaches and eskers (Class 6) correspond to sand and gravel beach (Mr) and esker (GFc) deposits as expected, along with till blanket (Tb) which is typically adjacent. However, at Site RI08, the majority of the area classified as beaches and eskers (Class 6) is mapped as T.M. This does not mean that all existing beaches and eskers are not correctly classified, but that a lot of ground may be incorrectly classified as Class 6. Closer inspection reveals that in areas of potential misclassification, what is mapped as T.M is actually washed till that may include littoral sediments and that has surface vegetation similar to that of more pronounced beaches and eskers.

Areas classified as dry polygonal ground (Class 7) are composed mostly of undifferentiated till and marine (T.M) and nearshore marine (Mn) sediments, whereas areas classified as wet polygonal ground (Class 8) are composed mostly of nearshore marine (Mn) sediments. Areas classified as dry patterned ground, till plain, and wet vegetation (Classes 9–11) all correspond mainly to undifferentiated till and marine (T.M) sediments, although areas of dry patterned ground (Class 9) have a significant component of till blanket (Tb), and areas of wet vegetation (Class 11) have a significant component of nearshore marine (Mn) sediments that tend to occupy topographic lows. Finally, at Site RI08, areas classified as bedrock (Class 12) correspond mostly to undifferentiated bedrock (R), but also to undifferentiated till and marine (T.M) sediments. This may be a result of the dark spectral signatures of these areas, combined with their presence on topographic highs typical of bedrock.

DISCUSSION

The MS+T+TPI feature set is accepted as generating the most reliable permafrost terrain classification in terms of accuracy, visual inspection, and correspondence to surficial geology. Overall accuracy is encouraging, but there is still significant misclassification and confusion across classes as evidenced by the confusion matrices (Appendices A and B). The population proportional TPR, PPV and confusion descriptors are summarized in Tables 4 and 5 for the MS+T+TPI feature set at Sites RI05 and RI08, respectively.

Further improvements in classification accuracy (a reduction in misclassification) may be achieved by grouping classes that exhibit confusion. For example, Classes 5, 7, and 8 exhibit a large amount of inter-class confusion (Table 4), but are all defined as medium to high thaw sensitivity, despite their more nuanced differences (Table 1). Merging these classes results in almost all ground that was classified as Class 5, 7, or 8 being classified as the new merged class, which removes the previous inter-class confusion and improves average TPR and PPV for both sites. Similarly, merging Classes 10 and 11 improves average TPR and PPV (to a lesser degree) and reduces the observed inter-class confusion, but these classes have disparate thaw sensitivities (Table 1), such that important information is lost in the resulting map. In contrast, merging Classes 5 and 11 results in decreased average accuracy for both sites. This is because despite their similarity as wet ground, they exhibit only a small amount of confusion in classification, and much of what was classified as Class 5 gets classified as Class 8 rather than the new merged class. The reduced confusion due to merging is outweighed by a loss in the degrees of freedom for the classification.

In the context of permafrost conditions and thaw sensitivity, some confusion is acceptable between classes with similar characteristics, and some confusion is necessary to maintain separation between classes with disparate characteristics. At the expense of lower average accuracy, all classes are kept separate to retain the higher degree of fidelity. In the case of Classes 5, 7, 8, and 11, some misclassification may occur as detailed in Tables 4 and 5, but it is of limited consequence, and the group accuracy is higher than that of the individual classes. Conversely, Classes 10 and 11 are similar in terms of surficial geology, but have different thaw sensitivity. In this case, keeping these classes separate forces as much distinction as the data allow, but the confusion between these classes is of much greater concern and must be carefully considered. In all cases, the increase in average accuracy obtained by merging classes is not nearly as large as that obtained by introducing texture or TPI to the classification.

CONCLUSION

Permafrost terrain classification was possible using Multispectral WorldView-2 satellite imagery at two study sites inland of the Hamlet of Rankin Inlet, Nunavut, where the reference classification was based on observed permafrost conditions and inferred thaw sensitivity. The 4-band multispectral data alone provide a moderate level of prediction accuracy (62–80% TPR and PPV over both sites). Prediction accuracy is improved significantly by addition of the derivative image feature of texture, and the independent variable of topographic position (85–95% TPR and PPV over both sites). Merging classes demonstrates that certain classes with common permafrost characteristics can be considered together with improved accuracy. Improved accuracy for merged classes gives confidence that the data are not over-fit with too many classes, and that improved fidelity of more classes can be accepted at the expense of lower accuracy.

In general, the expected correspondence between permafrost terrain classification and surficial geology is good, and is improved by addition of texture and TPI, but this is not easily quantified. Unexpected discrepancy between the permafrost terrain classification and surficial geology may be explained by lower-resolution geological maps, or by common vegetation types resulting in spectral overlap, or topographic and/or textural non-uniqueness.

Uncertainty in the classifications is addressed using a confusion descriptor that describes the likelihood of a particular class being misclassified, or incorrectly predicted in the presence of another class. The confusion descriptor is particularly important for classes that may exhibit similar spectral and topographic characteristics, but that are associated with different permafrost conditions and implications for thaw subsidence. Improved accuracy may be achieved using other classifiers better suited for noisy data or non-Gaussian image variables. Similarly, classifiers suitable for the incorporation of categorical data such as geology may prove useful.

ACKNOWLEDGEMENTS

Part of the Natural Resources Canada Climate Change Geoscience Program. Additional support provided by the Canada-Nunavut Geoscience Office, Canada. Valuable assistance provided by: R. Connelly, Government of Nunavut, Department of Economic Development and Transportation; S. Napier, formerly Nunavut Arctic College; A. Netser, Nunavut Arctic College; D. Beamer, formerly Government of Nunavut, Department of Environment. Interpretation of superficial geology provided by I. McMartin. Field assistance from O. Bellehumeur-Génier and N. Ymana. Internal review by M. Ednie. Topographic Data from Natural Resources Canada (http://open.canada.ca/en/open-maps).

REFERENCES

Andén J., Mallat S., 2014. Deep Scattering Spectrum. IEEE Transactions on Signal Processing 62, 4114–4128.

Behnia P., Harris J.R., Rainbird R.H., Williamson M.C., Sheshpari M., 2012. Remote predictive mapping of bedrock geology using image classification of Landsat and SPOT data, western Minto Inlier, Victoria Island, Northwest Territories, Canada. International Journal of Remote Sensing 33, 6876–6903.

Campbell J.E., Harris J.R., Huntley D.H., McMartin I., Wityk U., Dredge L.A., Eagles S., 2013. Remote Predictive Mapping of Surficial Earth Materials: Wager Bay North Area, Nunavut - NTS 46-E (N), 46-K (SW), 46-L, 46-M (SW), 56-H (N), 56-I and 56-J (S). Geological Survey of Canada, Open File 7118.

Drury S. A., 1993. Image Interpretation in Geology, 2nd Edition. Chapman and Hall.

Dyke A.S., 2004. An outline of North American deglaciation with emphasis on central and northern Canada. Developments in Quaternary Science 2, 373–424.

French H., Shur Y., 2010. The principles of cryostratigraphy. Earth Science Reviews 101, 190–206.

Foody G.M., 2002. Status of land cover classification accuracy assessment. Remote Sensing of Environment 80, 185–201.

Grunsky E., Harris J.R., McMartin I., 2006. Predictive mapping of surficial materials, Shultz Lake area (NTS 66A), Nunavut, Canada. Geological Survey of Canada, Open File 5153.

GSC, 2017. Surficial geology, Rankin Inlet, Nunavut, NTS 55-K/16. Geological Survey of Canada, Canadian Geoscience Map 68.

Guisan A., Weiss S.B., Weiss A.D., 1999. GLM versus CCA spatial modeling of plant species distribution. Plant Ecology 143, 107–122.

Hammond T.O., Verbyla D.L., 1996. Optimistic bias in classification accuracy assessment, International Journal of Remote Sensing 17, 1261–1266.

He, J. Harris J.R., Sawada M., Behnia P., 2015. A comparison of classification algorithms using Landsat-7 and Landsat-8 data for mapping lithology in Canada’s Arctic. International Journal of Remote Sensing 36, 2252–2276.

Heginbottom J.A., Dubreuil M.H., Harker P.T., 1995. Canada, Permafrost. National Atlas of Canada, 5th ed., Plate 2.1, MCR 4177.

Hogland J., Billor N., Anderson N., 2013. Comparison of standard maximum likelihood classification and polytomous logistic regression used in remote sensing; European Journal of Remote Sensing, 46, 623–640.

Humeau-Heurtier A., 2019. Texture feature extraction methods: survey. IEEE Access 7, 8975–9000.

Hung J.K.Y., Treitz P., 2020. Environmental land-cover classification for integrated watershed studies: Cape Bounty, Melville Island, Nunavut. Arctic Science 6, 404–422.

LeBlanc A.-M., Bellehumeur-Génier O., Oldenborger G.A., Short N., 2020. Lake area and shoreline changes due to climate and permafrost-related drivers, Rankin Inlet area, Nunavut. Canada-Nunavut Geoscience Office, Summary of Activities 2019, 79–92.

LeBlanc A.-M., Oldenborger G.A., 2021. Ground temperature, active layer thickness and ground ice conditions in the vicinity of Rankin Inlet, Nunavut. Canada-Nunavut Geoscience Office, Summary of Activities 2020, 63–72.

LeBlanc A.-M., Oldenborger G. A., Short N., 2019. Mapping permafrost and terrain conditions by combining corrected DInSAR seasonal and inter-annual ground displacements, Proceedings of the Canadian Permafrost Conference, 616–624.

Lillesand T., Kiefer R.W., Chipman J., 2015. Remote Sensing and Image Interpretation, 7th Edition. John Wiley & Sons.

LaRocque A., Leblon B., Harris J., Jefferson C., Tschirhart V., Shelat Y., 2012. Surficial materials mapping in Nunavut, Canada with multibeam RADARSAT-2 dual-polarization CHH and C-HV, LANDSAT-7 ETM+, and DEM data. Canadian Journal of Remote Sensing 38, 281–305.

McMartin I., 2002. Surficial geology, Rankin Inlet, Nunavut. Geological Survey of Canada, Open File 4116.

Morin P., Porter C., Cloutier M., Howat I., Noh M.-J., Willis M., Bates B., Willamson C., Peterman K., 2016. ArcticDEM: A publically available, high resolution elevation model of the Arctic. EGU General Assembly 18, 8396.

Oldenborger G.A., Bellehumeur-Génier O., Short N., Tremblay T., LeBlanc A.-M., 2017. Ground temperatures and permafrost conditions, Rankin Inlet, southern Nunavut. Canada-Nunavut Geoscience Office, Summary of Activities 2017, 117–128.

Oldenborger G.A., Schincariol R.A., Mansinha L., 2002. Space-local spectral texture segmentation applied to characterizing the heterogeneity of hydraulic conductivity. Water Resources Research 38, 1154.

Oldenborger G.A., Short N., LeBlanc A.-M., 2020. Electrical conductivity and ground displacement in permafrost terrain. Journal of Applied Geophysics 181, 104148.

Olthof I., Latifovic R., Pouliot D., 2009. Development of a circa 2000 land cover map of northern Canada at 30 m resolution from Landsat. Canadian Journal of Remote Sensing 35, 152–165.

O'Neill H.B., Wolfe S.A., Duchesne C., 2019. New ground ice maps for Canada using a paleogeographic modelling approach, The Cryoshpere 13, 753–773.

Stehman S.V., Foody G.M., 2019. Key issues in rigorous accuracy assessment of land cover products. Remote Sensing of Environment 231, 111199.

Williams A.T., Fulton R.J., Thomas M.C., 1998. Sand grain analysis—image processing, textural algorithms and neural nets. Computers & Geosciences 24, 111–118.

TABLES

Table 1. Permafrost terrain reference class descriptions and thaw sensitivity.

Class	Name	Thaw Sensitivity	Description
1	Deep water	Nil Shoreline: Low-High[1,2]	Large lakes, deep water bodies
2	Shallow water	Nil Shoreline: Low-High[1,2]	Small lakes, shallow water bodies, lake terraces
3	Exposed sand and gravel	Low	Freshly eroded or exposed sand and gravel sediments, raised beaches and eskers, trails
4	Dry water body	Med-High	Dried modern ponds, lake beds, and shorelines, bare of vegetation
5	Flooded vegetation	High[3]	Modern stream systems and wetlands, herbacious vegetation (grass) with ponded water or seasonal flooding, some peat
6	Beaches and eskers	Low[4]	Sand and gravel hills with dark vegetation (lichen), raised beaches and glaciofluvial (eskers), disconnected ice-wedge troughs
7	Dry polygonal ground	Med-High	Low-lying dry vegetation (shrub) in polygon centres, marine sediments
8	Wet polygonal ground	Med-High	Low-lying wet herbaceous vegetation (sedge, grass), connected ice-wedge troughs or seasonally flooded areas, marine sediments
9	Dry patterned ground	Low-Med	Dry vegetation (shrub) with mudboils and stone circles, till blanket
10	Till plain	Low	Tundra vegetation (shrub, grass, moss) over extensive till, some mudboils or exposed boulders
11	Wet vegetation	High	Hummocky ground with tussock vegetation and inter-hummock water, undifferentiated till and marine sediments
12	Bedrock	Nil	Outcrop or exposed rock (possibly subcrop or float)

[1]Subject to thermokarst and [2]potential lake drainage (LeBlanc et al., 2020)
[3]Prevelent seasonal frost blisters (LeBlanc and Oldenborger, 2021)
[4]Wedge ice present in disconnected troughs (Oldenborger et al., 2017)

Table 2. Permafrost terrain classification performance metrics for the different classes and feature sets at study site RI05.

Class	Name	MS		MS+T		MS+TPI		MS+T+TPI	
		TPR (%)	PPV (%)	TPR (%)	PPV (%)	TPR (%)	PPV (%)	TPR (%)	PPV (%)
1	Deep water	93.8	76.7	89.4	100	93.0	99.0	88.7	100
2	Shallow water	98.1	99.7	99.6	99.5	99.6	99.6	99.8	99.4
3	Exposed sand and gravel	91.9	96.6	94.6	96.4	96.9	97.5	98.9	98.1
4	Dry water body	88.8	49.5	96.4	70.3	99.4	73.8	99.5	85.6
5	Flooded vegetation	57.3	48.5	69.0	77.5	68.0	68.7	76.2	84.4
6	Beaches and eskers	76.0	65.6	94.2	79.7	90.9	76.0	94.4	81.8
7	Dry polygonal ground	54.3	23.4	66.1	28.4	82.5	55.2	86.0	59.4
8	Wet polygonal ground	72.1	27.1	80.8	53.0	84.6	51.3	91.0	67.9
9	Dry patterned ground	58.8	81.7	81.7	92.6	81.2	91.0	88.3	95.0
10	Till plain	66.0	74.3	71.7	85.3	75.0	88.0	81.4	92.2
11	Wet vegetation	39.1	43.9	70.8	61.6	75.3	66.1	87.9	73.3
12	Bedrock	NA	NA	NA	NA	NA	NA	NA	NA
	Average:	72.4	62.4	83.1	76.7	86.1	78.8	90.2	85.2

Table 3. Permafrost terrain classification performance metrics for the different classes and feature sets at study site RI08.

Class	Name	MS		MS+T		MS+TPI		MS+T+TPI	
		TPR (%)	PPV (%)	TPR (%)	PPV (%)	TPR (%)	PPV (%)	TPR (%)	PPV (%)
1	Deep water	99.2	99.7	98.8	99.8	99.0	99.8	98.9	99.8
2	Shallow water	98.6	99.3	99.0	99.0	98.9	99.7	99.0	99.6
3	Exposed sand and gravel	98.6	99.5	98.8	99.6	98.7	99.5	99.0	99.6
4	Dry water body	98.2	58.3	98.4	68.0	98.3	64.1	98.6	67.6
5	Flooded vegetation	67.7	76.9	81.3	85.8	90.7	98.1	95.8	98.9
6	Beaches and eskers	80.1	66.4	81.3	74.7	85.5	73.5	90.1	79.4
7	Dry polygonal ground	53.1	7.3	74.8	21.6	83.9	39.4	92.5	54.3
8	Wet polygonal ground	82.0	47.5	86.3	79.7	90.8	92.0	92.4	93.1
9	Dry patterned ground	42.4	80.2	85.4	91.5	91.7	97.4	92.8	97.4
10	Till plain	65.6	66.8	70.8	79.4	93.5	90.1	94.8	91.3
11	Wet vegetation	83.7	65.4	85.6	76.7	91.3	84.4	94.6	93.4
12	Bedrock	93.4	65.7	94.1	69.9	93.8	45.3	94.4	48.1
	Average:	80.2	69.4	87.9	78.8	93.0	81.9	95.2	85.2

Table 4. Summary of permafrost terrain classification performance metrics and confusion descriptors for the MS+T+TPI feature set at Site RI05.

Class	Name	TPR (%)	PPV (%)	TPR (%)*	Confusion
1	Deep water	88.7	100	55.5	Often mapped as Class 2
2	Shallow water	99.8	99.4	98.8	Rarely mapped as Class 4; rarely confused with Class 1
3	Exposed sand and gravel	98.9	98.1	98.0	Rarely mapped as Class 4 and 6; rarely confused with Class 6
4	Dry water body	99.5	85.6	99.4	Sometimes confused with Class 2, rarely confused with Class 3, 11, and 5
5	Flooded vegetation	76.2	84.4	65.4	Sometimes mapped as Class 7, 8, and 11, rarely mapped as Class 10; sometimes confused with Class 10, rarely confused with Class 11, 8, and 7
6	Beaches and eskers	94.4	81.8	89.9	Sometimes mapped as Class 9; sometimes confused with Class 9
7	Dry polygonal ground	86.0	59.4	92.4	Rarely mapped as Class 5, 11, 10 and 8; sometimes confused with Class 10 and 5; rarely confused with Class 11, 8, and 2
8	Wet polygonal ground	91.0	67.9	87.2	Sometimes mapped as Class 5, rarely mapped as Class 7 and 11; sometimes confused with Class 5, rarely confused with Class 7 and 11
9	Dry patterned ground	88.3	95.0	92.1	Rarely mapped as Class 6 and 10; rarely confused with Class 10 and 6
10	Till plain	81.4	92.2	78.1	Sometimes mapped as Class 11 and 7, rarely mapped as Class 9 and 5; rarely confused with Class 9, 11, and 5
11	Wet vegetation	87.9	73.3	91.8	Sometimes mapped as Class 10, rarely mapped as Class 5, 7, and 9; sometimes confused with Class 10, rarely confused with Class 5, 7, and 2
12	Bedrock	NA	NA	NA	NA
	Average:	90.2	85.2	86.2	

*Based on prevalence-weighted population proportional area

Table 5. Summary of permafrost terrain classification performance metrics and confusion descriptors for the MS+T+TPI feature set at Site RI08.

Class	Name	TPR (%)	PPV (%)	TPR (%)*	Confusion
1	Deep water	98.9	99.8	90.3	Sometimes mapped as Class 12, rarely mapped as Class 2
2	Shallow water	99.0	99.6	97.0	Rarely mapped as Class 4 and 8
3	Exposed sand and gravel	99.0	99.6	96.7	Rarely mapped as Class 6
4	Dry water body	98.6	67.6	95.2	Rarely mapped as Class 6 and 7; sometimes confused with Class 2, rarely confused with Class 3
5	Flooded vegetation	95.8	98.9	76.9	Sometimes mapped as Class 7, rarely mapped as Class 6 and 11; rarely confused with Class 8
6	Beaches and eskers	90.1	79.4	97.5	Rarely mapped as Class 12 and 9; sometimes confused with Class 9 and 10; rarely confused with Class 5 and 12
7	Dry polygonal ground	92.5	54.3	98.8	Rarely mapped as Class 11; sometimes confused with Class 8, 5 and 11; rarely confused with Class 10
8	Wet polygonal ground	92.4	93.1	69.6	Sometimes mapped as Class 7, rarely mapped as Class 11 and 5; rarely confused with Class 2, 11, and 5
9	Dry patterned ground	92.8	97.4	72.4	Sometimes mapped as Class 6 and 10, rarely mapped as Class 12; rarely confused with Class 10 and 6
10	Till plain	94.8	91.3	94.8	Rarely mapped as Class 6 and 9; sometimes confused with Class 10, rarely confused with Class 11
11	Wet vegetation	94.6	93.4	88.4	Sometimes mapped as Class 7, rarely mapped as Class 10 and 8; rarely confused with Class 5, 8, and 10
12	Bedrock	94.4	48.1	83.8	Sometimes mapped as Class 6; often confused with Class 1, sometimes confused with Class 6 and 9
	Average:	95.2	85.2	88.5	

*Based on prevalence-weighted population proportional area

FIGURES

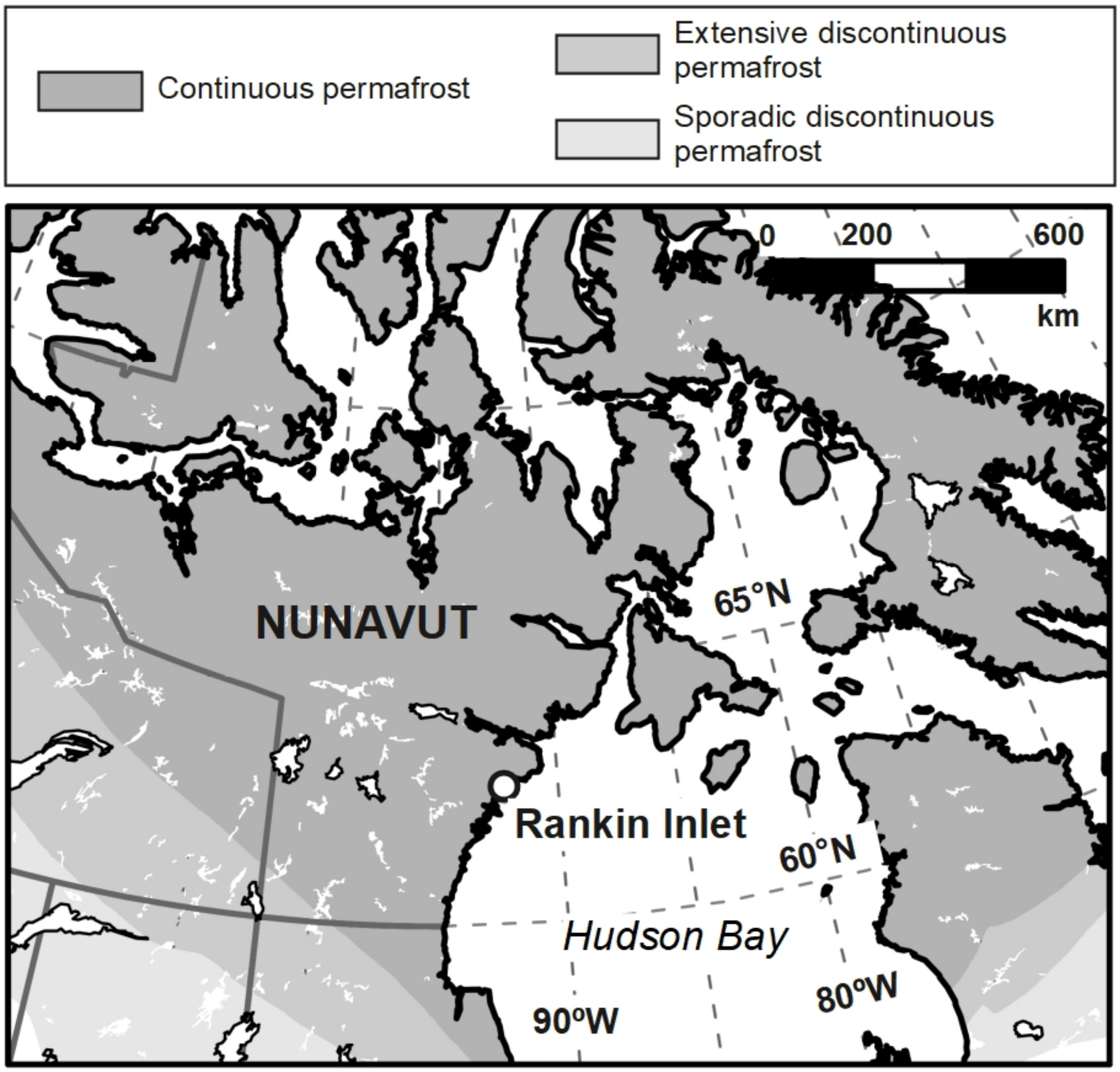

Figure 1. a) Location of Rankin Inlet, Nunavut and permafrost distribution in the Hudson Bay region of northern Canada (Heginbottom et al., 1995).

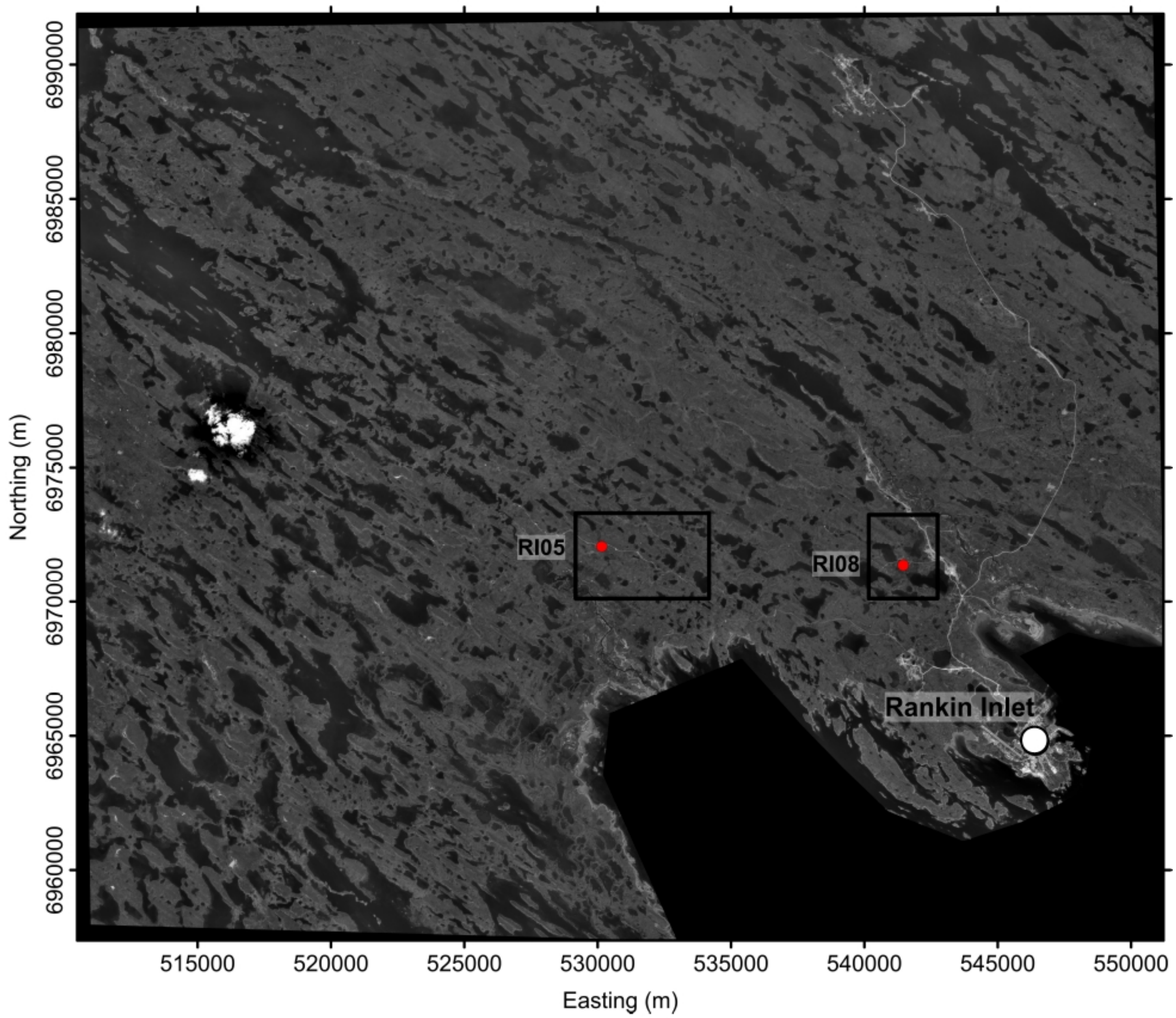

Figure 2. Luminosity-preserved greyscale composite of the orthorectified and corrected multispectral WorldView-2 mosaic, and locations of study sites RI05 (15 km^2) and RI08 (7 km^2). Markers within the study areas indicate borehole and ground temperature measurement locations.

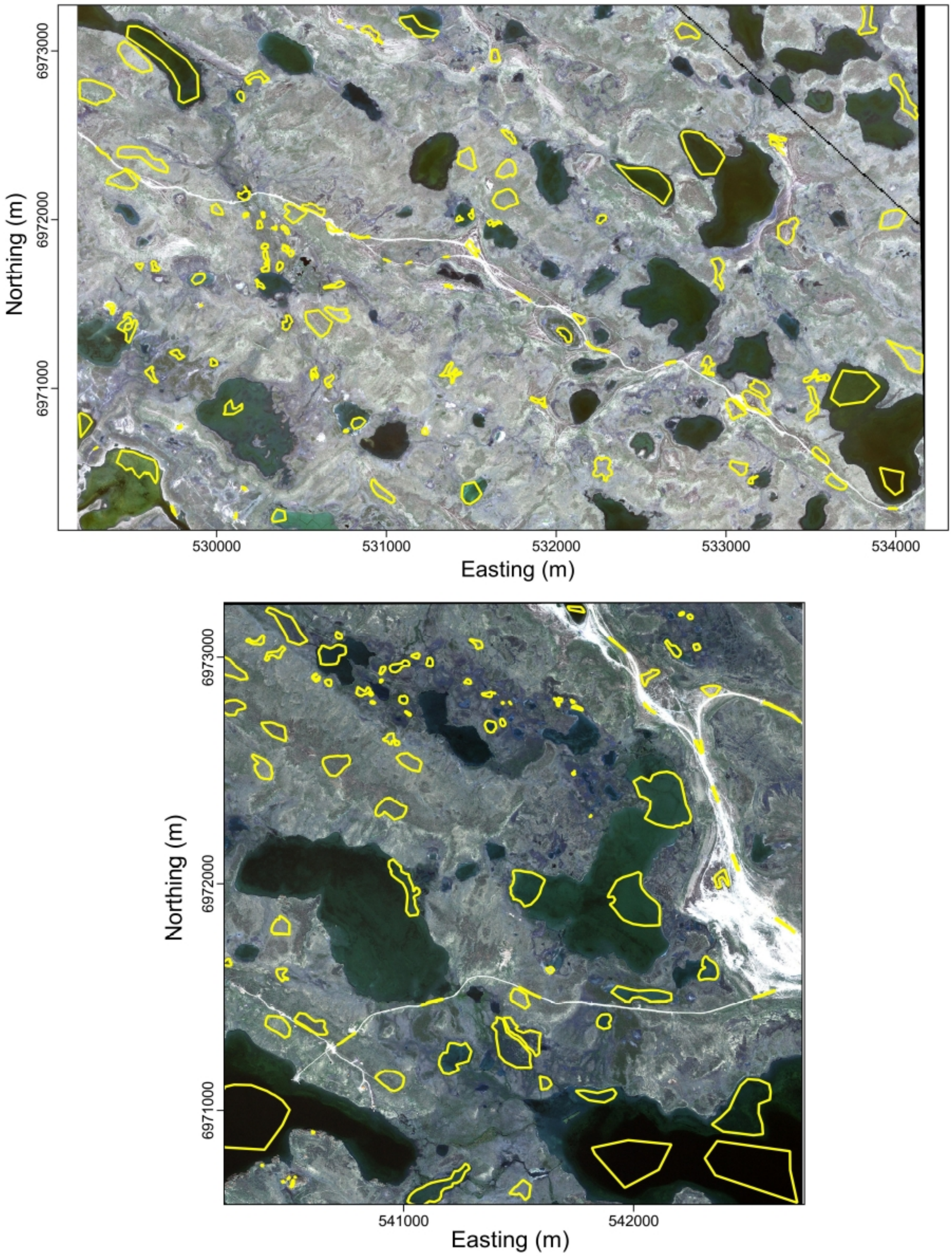

Figure 3. Reference classifications for sites RI05 (top) and RI08 (bottom) shown in true colour composite. The linear feature across the northeast portion of RI05 results from a gap in the panchromatic data from which the pansharpened image is derived.

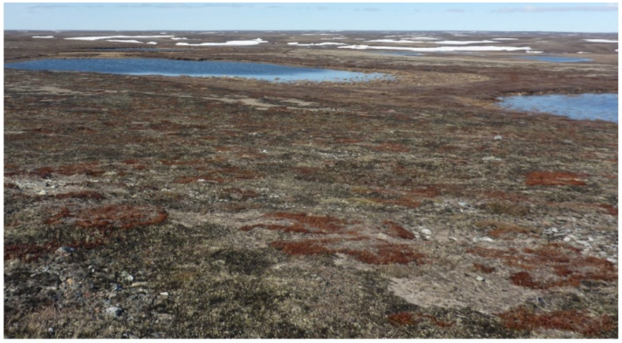

Photo of esker (Class 6) and exposed sand and gravel (Class 3) by A.M. LeBlanc. NRCan photo 2021-007

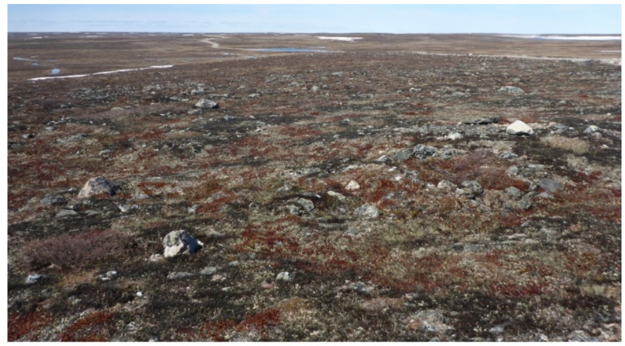

Photo of dry patterned ground (Class 9) by A.M. LeBlanc. NRCan photo 2021-012

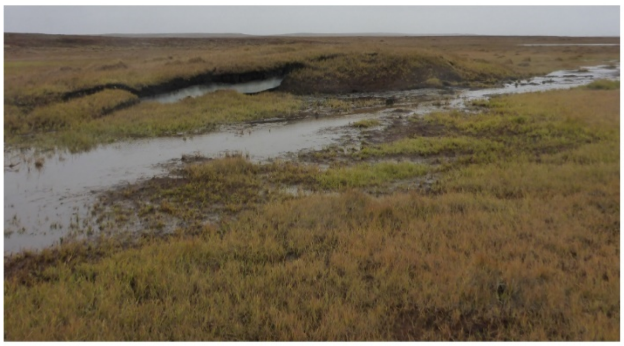

Photo of flooded vegetation (Class 5) by A.M. LeBlanc. NRCan photo 2021-009

Photo of till plain (Class 10) by A.M. LeBlanc. NRCan photo 2021-008

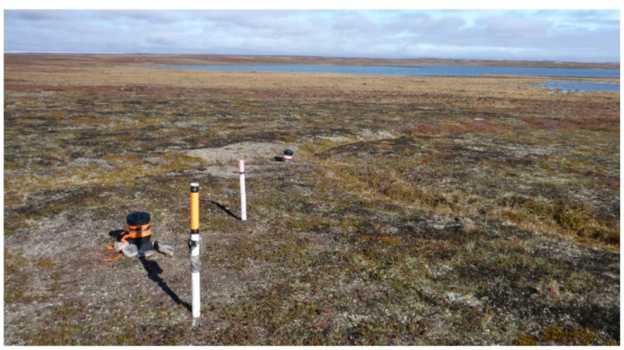

Photo of beach (Class 6) by A.M. LeBlanc. NRCan photo 2021-011

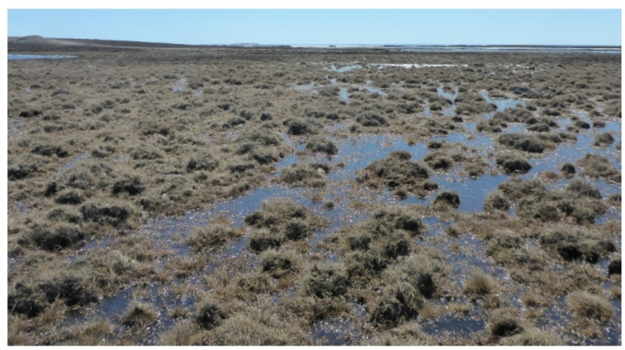

Photo of wet vegetation (Class 11) by A.M. LeBlanc. NRCan photo 2021-013

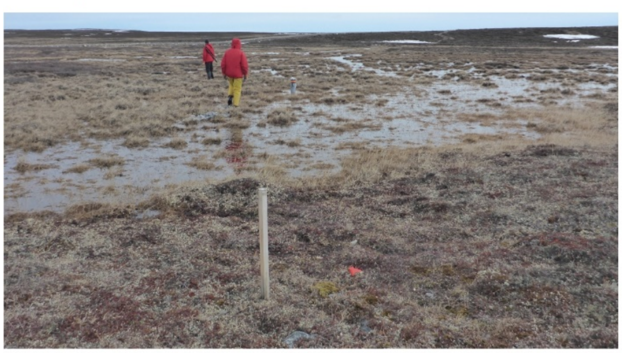

Photo of dry and wet polygonal ground (Classes 7 and 8) by A.M. LeBlanc. NRCan photo 2021-010

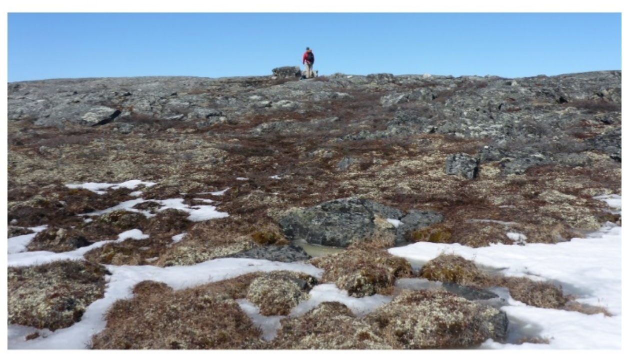

Photo of bedrock (Class 12) by A.M. LeBlanc. NRCan photo 2021-014

Figure 4. Example on-the-ground photographs for a selection of reference classes.

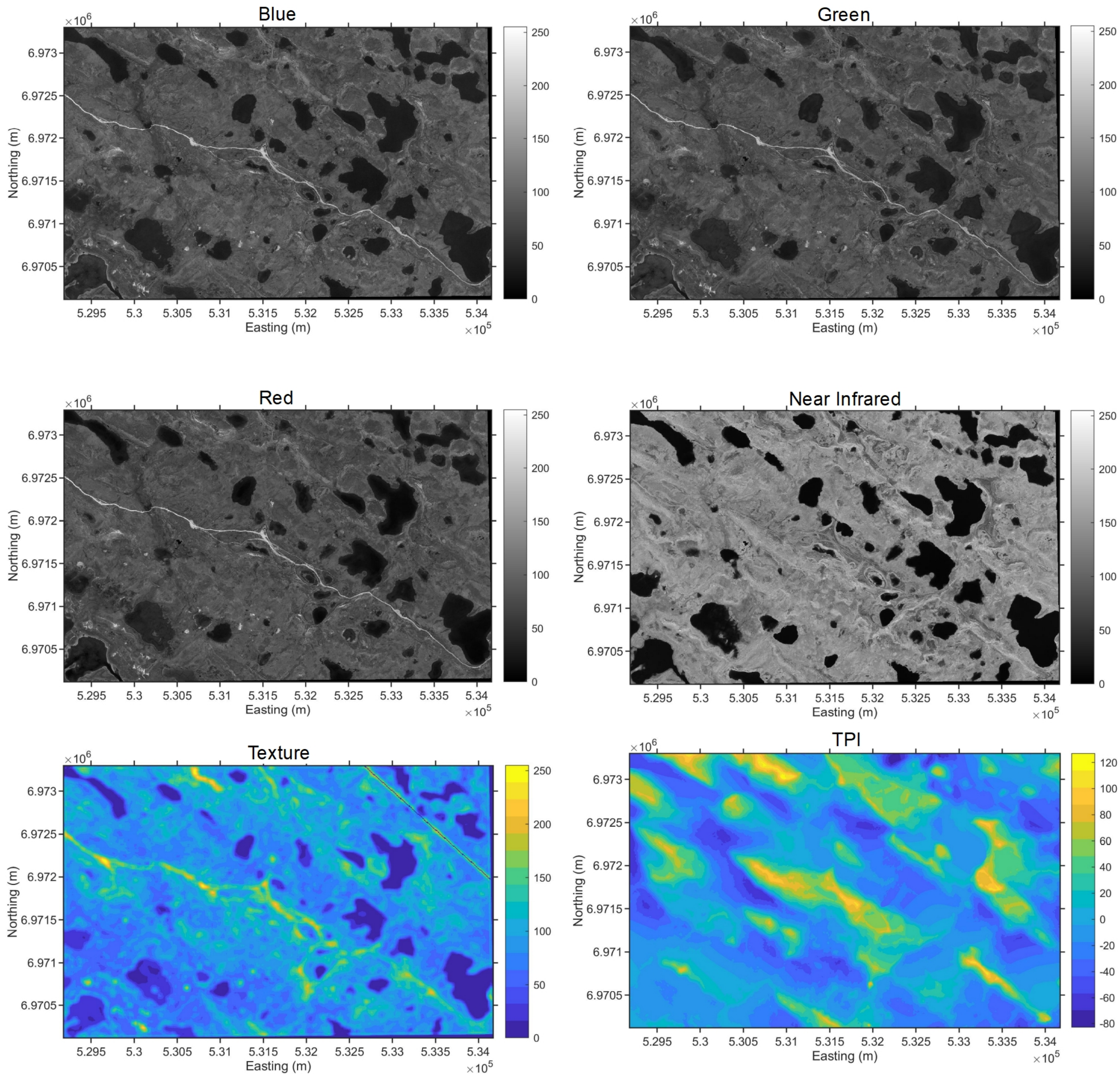

Figure 5. Feature set for site RI05. The linear feature across the northeast portion of the texture map results from a gap in the panchromatic data from which texture is derived.

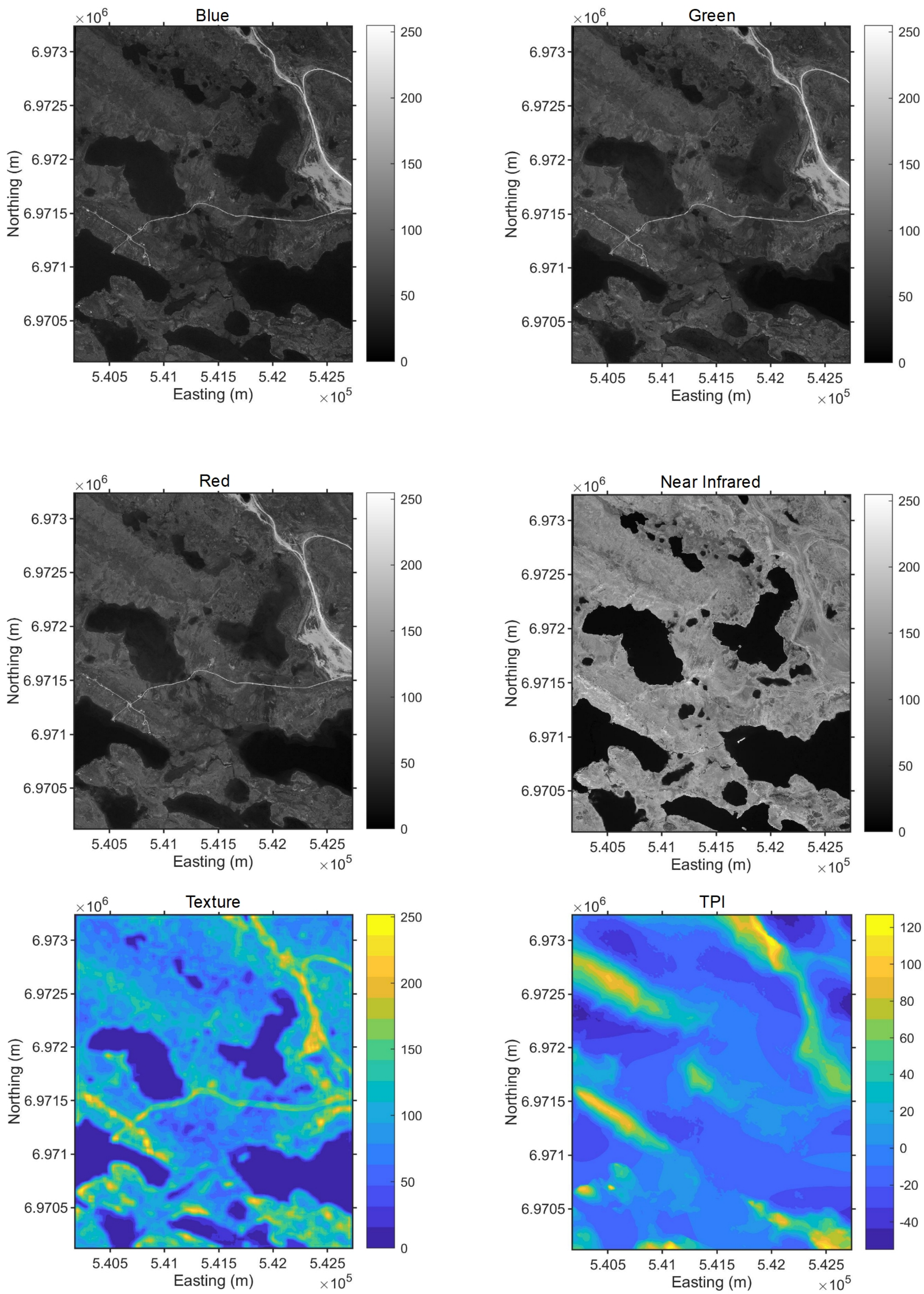

Figure 6. Feature set for site RI08.

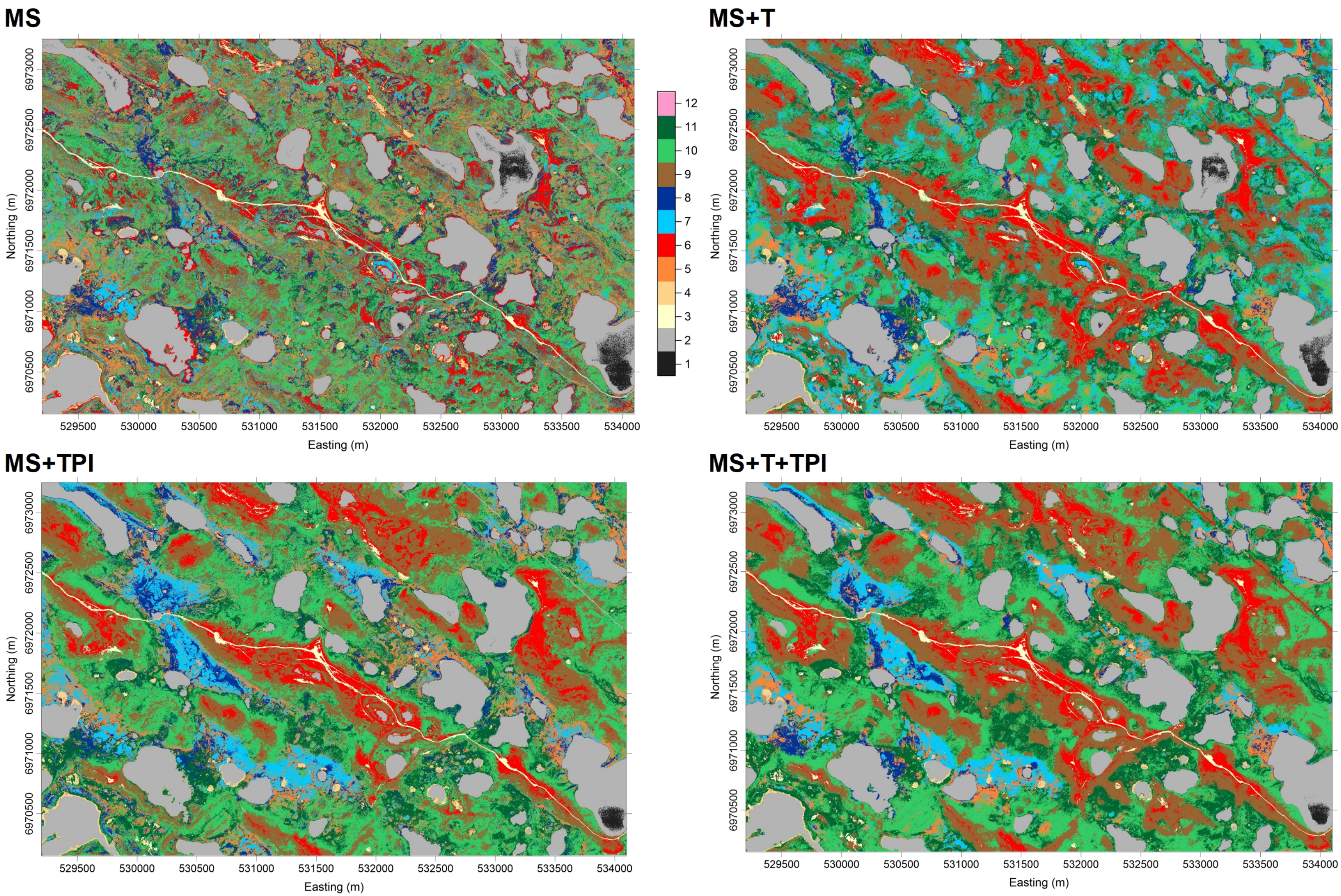

Figure 7. Site RI05 permafrost terrain classifications for the four different feature sets.

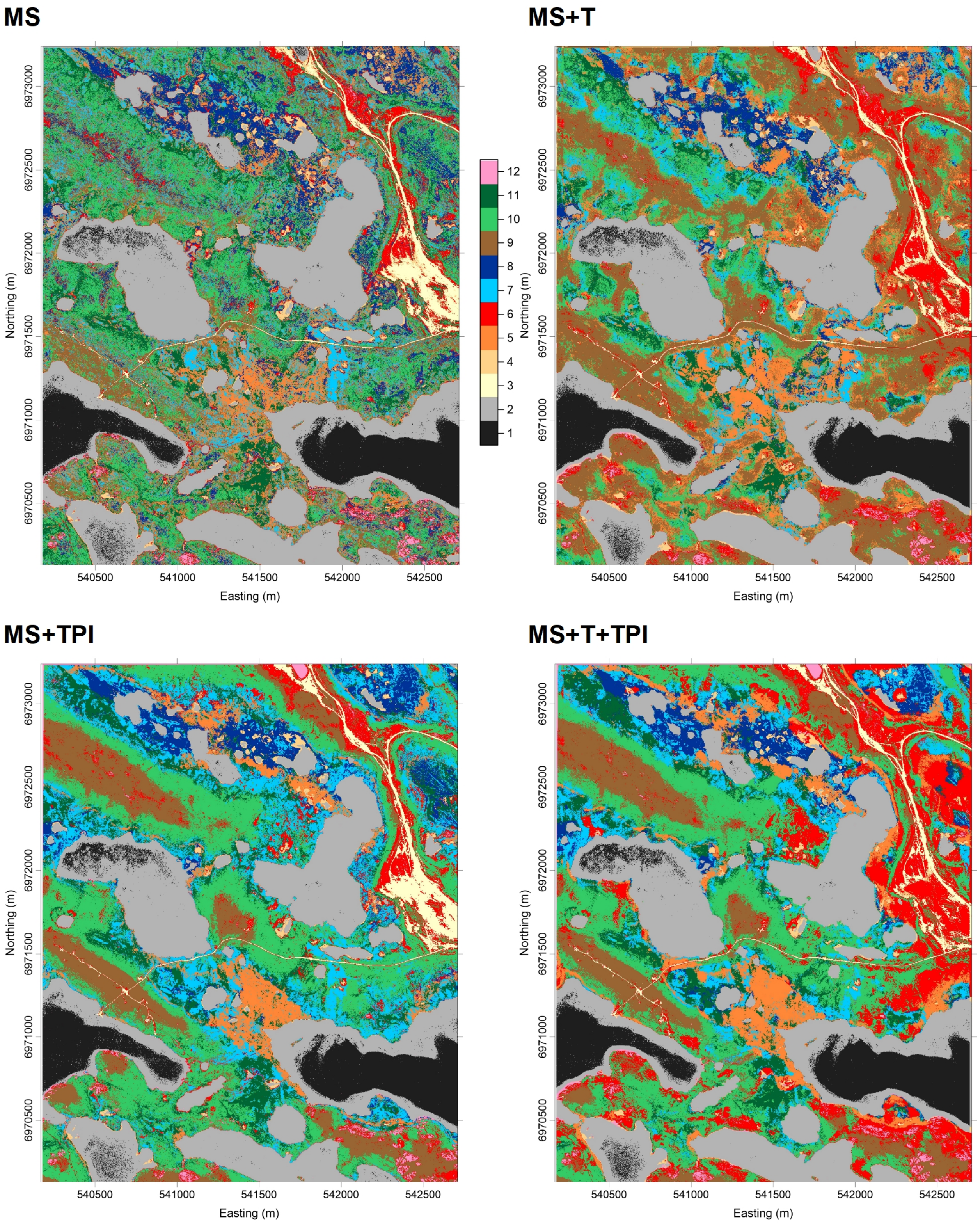

Figure 8. Site RI08 permafrost terrasin classifications for the four different feature sets.

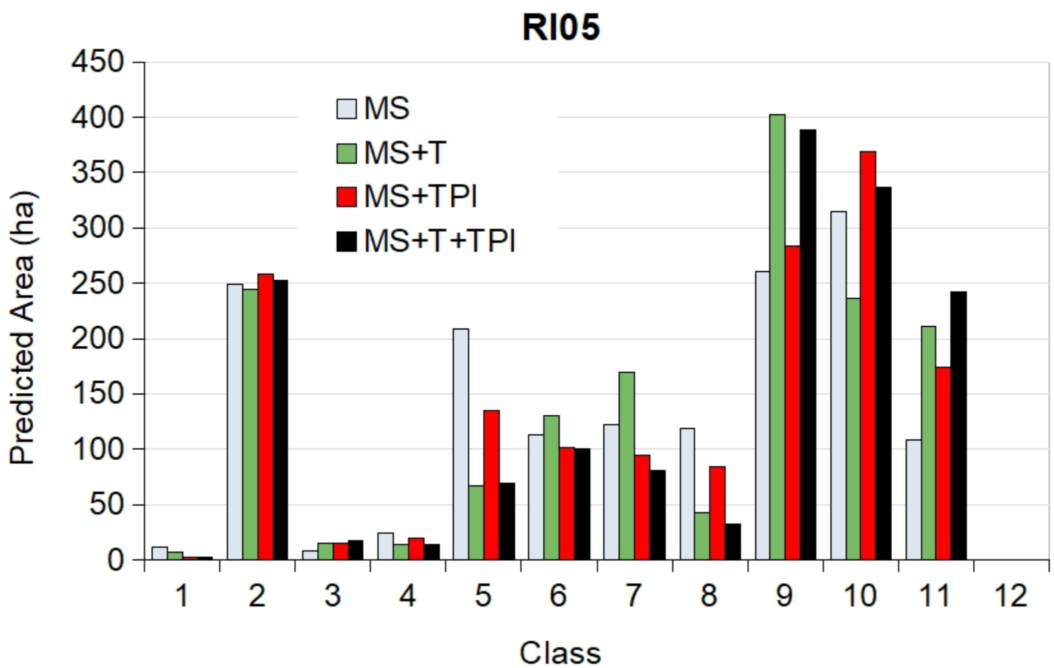

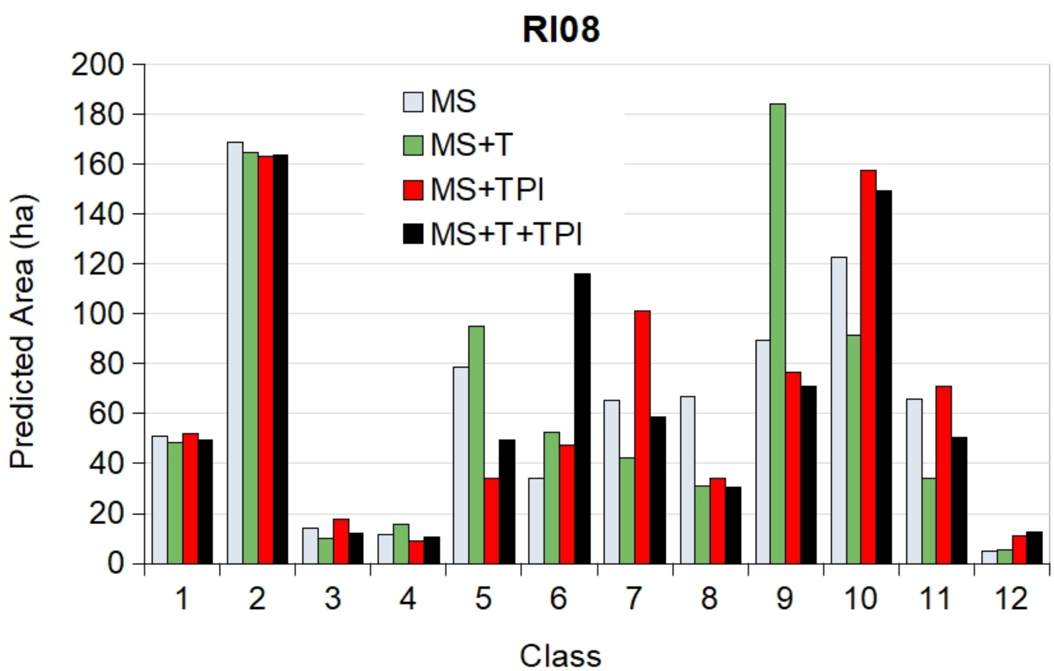

Figure 9. Predicted class areas over study sites RI05 and RI08 for the four different feature sets.

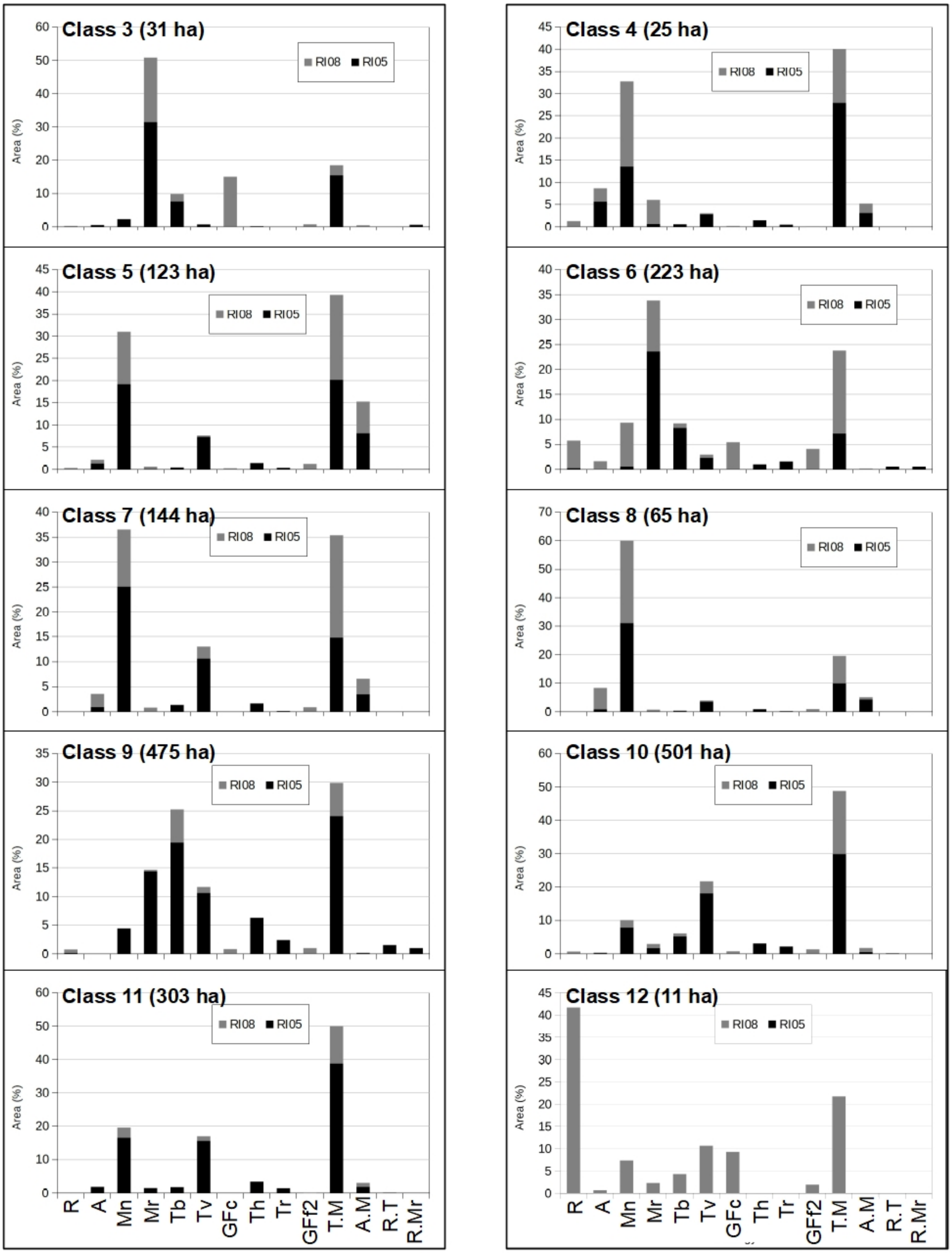

Figure 10. Distribution of surficial geology for each permafrost terrain class at sites RI05 and RI08 combined for the M+T+TPI feature set. Surficial geology from GSC (2017).

APPENDIX A

Study Site RI05
MS

Confusion Matrix (% Reference Class)

Reference	Predicted 1	2	3	4	5	6	7	8	9	10	11	12	Sum	Reference Pixels	Prevalence % Reference	Predicted Pixels	Prevalence % Map	Predicted Area (ha)
1	93.81	6.19	0.00	0.00	0.00	0.00	0.00	0.00	0.00	0.00	0.00		100.0	53691	2.26	475377	0.77	11.88
2	1.49	98.06	0.00	0.28	0.00	0.16	0.00	0.00	0.00	0.00	0.01		100.0	1029707	43.33	9954240	16.18	248.86
3	0.00	0.00	91.86	7.10	0.00	0.26	0.76	0.00	0.00	0.02	0.00		100.0	38365	1.61	338156	0.55	8.45
4	0.00	0.00	10.66	88.84	0.01	0.07	0.37	0.00	0.00	0.00	0.06		100.0	10135	0.43	953422	1.55	23.84
5	0.00	0.00	0.00	0.05	57.26	0.47	3.55	13.57	6.57	6.07	12.47		100.0	127920	5.38	8334293	13.55	208.36
6	0.00	0.00	0.09	1.82	0.25	75.95	0.71	5.29	3.04	7.62	5.22		100.0	163466	6.88	4516154	7.34	112.90
7	0.00	0.00	0.00	0.00	6.84	0.44	54.30	2.87	10.15	17.38	8.03		100.0	34220	1.44	4876559	7.93	121.91
8	0.00	0.00	0.00	0.00	9.22	3.82	0.58	72.05	3.66	1.87	8.79		100.0	41618	1.75	4748402	7.72	118.71
9	0.00	0.00	0.00	0.10	6.54	9.82	10.08	5.32	58.76	8.65	0.73		100.0	395619	16.65	10426384	16.95	260.66
10	0.00	0.00	0.00	0.00	6.74	3.12	3.81	1.66	8.93	66.03	9.71		100.0	346229	14.57	12568514	20.43	314.21
11	0.00	0.00	0.00	0.12	16.20	8.36	1.20	19.80	2.13	13.12	39.07		100.0	135278	5.69	4317422	7.02	107.94
12													0.0	0	0.00	0	0.00	0.00
SUM:	95.30	104.25	102.61	98.31	103.06	102.47	75.36	120.56	93.24	120.76	84.09	0.00		2376248	100	61508923	100	1538
NC:	11													**% Map**				
Avg TPR:	0.724													3.86				
Acc:	0.785																	

Confusion Matrix (Pixels*) *Subject to round-off error associated with calculating pixels from % reference class with 2 decimal places

Reference	Predicted 1	2	3	4	5	6	7	8	9	10	11	12	Support	N	TP	FN	TPR	PPV	FNR	F1
1	50368	3323	0	0	0	0	0	0	0	0	0	0	53691	2322554	50368	3323	0.938	0.767	0.062	0.844
2	15343	1009731	0	2883	0	1648	0	0	0	0	103	0	1029707	1346538	1009731	19976	0.981	0.997	0.019	0.989
3	0	0	35242	2724	0	100	292	0	0	8	0	0	38365	2337880	35242	3123	0.919	0.966	0.081	0.942
4	0	0	1080	9004	1	7	37	0	0	0	6	0	10136	2366109	9004	1132	0.888	0.495	0.112	0.635
5	0	0	0	64	73247	601	4541	17359	8404	7765	15952	0	127933	2248312	73247	54686	0.573	0.485	0.427	0.525
6	0	0	147	2975	409	124152	1161	8647	4969	12456	8533	0	163450	2212795	124152	39297	0.760	0.656	0.240	0.704
7	0	0	0	0	2341	151	18581	982	3473	5947	2748	0	34223	2342021	18581	15642	0.543	0.234	0.457	0.327
8	0	0	0	0	3837	1590	241	29986	1523	778	3658	0	41614	2334631	29986	11628	0.721	0.271	0.279	0.394
9	0	0	0	396	25873	38850	39878	21047	232466	34221	2888	0	395619	1980626	232466	163153	0.588	0.817	0.412	0.683
10	0	0	0	0	23336	10802	13191	5747	30918	228615	33619	0	346229	2030016	228615	117614	0.660	0.743	0.340	0.699
11	0	0	0	162	21915	11309	1623	26785	2881	17748	52853	0	135278	2240967	52853	82425	0.391	0.439	0.609	0.414
12	0	0	0	0	0	0	0	0	0	0	0	0	0	2376245	0	0				
Sum:	65710	1013054	36470	18208	150959	189210	79547	110553	284636	307539	120360	0	2376245							
FP:	15343	3323	1228	9204	77712	65057	60965	80568	52170	78924	67507	0				Avg:	0.724	0.624	0.276	0.651
TN:	2307211	1343214	2336652	2356905	2170600	2147738	2281056	2254063	1928456	1951092	2173460	2376245				Acc:	0.785			

N	Negatives	Number of negatives for class
TP	True Positive	Number of pixels correctly predicted as x for class x
FN	False Negative	Number of pixels incorrectly predicted as not x for class x
FP	False Positive	Number of pixels incorrectly predicted as x for not class x
TN	True Negative	Number of pixels correctly predicted as not x for not class x
TPR	True Positive Rate (Producer's Accuracy or Recall)	How often is x predicted for class x (conditional probability of correct prediction)
PPV	Positive Predictive Value (User's Accuracy or Precision)	How often the prediction of x is correct (posterior probability of correct prediction)
FNR	False Negative Rate	How often not x is predicted for class x
Acc	Accuracy	How often the classification is correct
F1	F1 Score	Harmonic mean of TPR and PPV

A1. RI05 MS confusion matrix, prevalence, and performance metrics.

Study Site RI05
MS+T

Confusion Matrix (% Reference Class)

Reference	Predicted 1	2	3	4	5	6	7	8	9	10	11	12	Sum	Reference Pixels	Prevalence % Reference	Predicted Pixels	Prevalence % Map	Predicted Area (ha)
1	89.44	10.56	0.00	0.00	0.00	0.00	0.00	0.00	0.00	0.00	0.00		100.0	53691	2.26	277254	0.45	6.93
2	0.00	99.59	0.03	0.20	0.00	0.01	0.00	0.01	0.12	0.00	0.05		100.0	1029707	43.33	9758891	15.87	243.97
3	0.00	0.00	94.61	4.30	0.00	0.20	0.88	0.00	0.01	0.00	0.00		100.0	38365	1.61	577038	0.94	14.43
4	0.00	0.00	3.31	96.36	0.01	0.00	0.25	0.00	0.00	0.00	0.08		100.0	10135	0.43	572374	0.93	14.31
5	0.00	0.00	0.00	0.04	69.01	0.01	3.91	14.23	0.09	3.99	8.73		100.0	127920	5.38	2672585	4.35	66.81
6	0.00	0.00	0.42	0.00	0.00	94.24	0.00	0.00	5.34	0.00	0.00		100.0	163466	6.88	5208915	8.47	130.22
7	0.00	0.00	0.00	0.00	3.19	0.02	66.15	4.39	3.61	17.64	5.01		100.0	34220	1.44	6781801	11.03	169.55
8	0.00	0.00	0.00	0.00	9.04	0.00	1.21	80.81	0.00	1.82	7.12		100.0	41618	1.75	1683631	2.74	42.09
9	0.00	0.00	0.01	0.00	0.00	9.41	5.18	0.00	81.66	3.03	0.70		100.0	395619	16.65	16071976	26.13	401.80
10	0.00	0.00	0.00	0.00	4.23	0.26	7.79	0.96	3.37	71.67	11.72		100.0	346229	14.57	9455183	15.37	236.38
11	0.00	0.00	0.00	0.27	4.55	0.76	2.70	4.94	2.11	13.88	70.79		100.0	135278	5.69	8449275	13.74	211.23
12													0.0	0	0.00	0	0.00	0.00
Sum:	89.44	110.15	98.38	101.17	90.03	104.91	88.07	105.34	96.31	112.03	104.20	0.00		2376248	100	61508923	100	1538
NC:	11													% Map				
Avg TPR:	0.831													3.86				
Acc:	0.877																	

Confusion Matrix (Pixels*) *Subject to round-off error associated with calculating pixels from % reference class with 2 decimal places

Reference	Predicted 1	2	3	4	5	6	7	8	9	10	11	12	Support	N	TP	FN	TPR	PPV	FNR	F1
1	48021	5670	0	0	0	0	0	0	0	0	0	0	53691	2322638	48021	5670	0.894	1.000	0.106	0.944
2	0	1025485	309	2059	0	103	0	103	1236	0	515	0	1029810	1346519	1025485	4325	0.996	0.995	0.004	0.995
3	0	0	36297	1650	0	77	338	0	4	0	0	0	38365	2337964	36297	2068	0.946	0.964	0.054	0.955
4	0	0	335	9766	1	0	25	0	0	0	8	0	10136	2366193	9766	370	0.964	0.703	0.036	0.813
5	0	0	0	51	88278	13	5002	18203	115	5104	11167	0	127933	2248396	88278	39655	0.690	0.775	0.310	0.730
6	0	0	687	0	0	154050	0	0	8729	0	0	0	163466	2212863	154050	9416	0.942	0.797	0.058	0.863
7	0	0	0	0	1092	7	22637	1502	1235	6036	1714	0	34223	2342105	22637	11587	0.661	0.284	0.339	0.398
8	0	0	0	0	3762	0	504	33632	0	757	2963	0	41618	2334711	33632	7986	0.808	0.530	0.192	0.640
9	0	0	40	0	0	37228	20493	0	323062	11987	2769	0	395579	1980749	323062	72517	0.817	0.926	0.183	0.868
10	0	0	0	0	14645	900	26971	3324	11668	248142	40578	0	346229	2030100	248142	98087	0.717	0.853	0.283	0.779
11	0	0	0	365	6155	1028	3653	6683	2854	18777	95763	0	135278	2241051	95763	39515	0.708	0.616	0.292	0.659
12	0	0	0	0	0	0	0	0	0	0	0	0	0	2376329	0	0				
Sum:	48021	1031155	37668	13892	113933	193406	79622	63446	348904	290804	155479	0	2376329							
FP:	0	5670	1370	4126	25656	39355	56985	29815	25841	42662	59715	0				Avg:	0.831	0.767	0.169	0.786
TN:	2322638	1340849	2336593	2362067	2222740	2173507	2285120	2304896	1954908	1987438	2181335	2376329				Acc:	0.877			

A2. RI05 MS+T confusion matrix, prevalence, and performance metrics.

Study Site RI05
MS+TPI

Confusion Matrix (% Reference Class)

	Predicted																	
Reference	**1**	**2**	**3**	**4**	**5**	**6**	**7**	**8**	**9**	**10**	**11**	**12**	**Sum**	**Reference Pixels**	**Prevalence % Reference**	**Predicted Pixels**	**Prevalence % Map**	**Predicted Area (ha)**
1	93.01	6.99	0.00	0.00	0.00	0.00	0.00	0.00	0.00	0.00	0.00		100.0	53691	2.26	107540	0.17	2.69
2	0.05	99.63	0.00	0.23	0.00	0.01	0.00	0.01	0.00	0.00	0.06		100.0	1029707	43.33	10339999	16.81	258.50
3	0.00	0.00	96.89	2.40	0.00	0.70	0.00	0.00	0.01	0.00	0.00		100.0	38365	1.61	592765	0.96	14.82
4	0.00	0.00	0.06	99.45	0.03	0.00	0.34	0.00	0.00	0.09	0.04		100.0	10135	0.43	800679	1.30	20.02
5	0.00	0.00	0.00	0.08	68.04	0.00	6.85	14.67	0.01	0.98	9.37		100.0	127920	5.38	5405960	8.79	135.15
6	0.00	0.00	0.53	0.00	0.00	90.88	0.00	0.00	6.58	2.00	0.00		100.0	163466	6.88	4034262	6.56	100.86
7	0.00	0.00	0.00	0.00	9.08	0.00	82.51	4.88	0.01	0.56	2.96		100.0	34220	1.44	3786818	6.16	94.67
8	0.00	0.00	0.00	0.02	7.71	0.00	2.93	84.58	0.12	0.09	4.54		100.0	41618	1.75	3359653	5.46	83.99
9	0.00	0.00	0.02	0.00	0.93	11.45	0.70	0.10	81.24	5.54	0.04		100.0	395619	16.65	11343808	18.44	283.60
10	0.00	0.00	0.00	0.00	5.10	0.33	2.62	0.44	5.90	75.04	10.57		100.0	346229	14.57	14776498	24.02	369.41
11	0.00	0.00	0.00	0.13	8.84	0.00	0.75	8.11	0.41	6.46	75.29		100.0	135278	5.69	6960941	11.32	174.02
12													0.0	0	0.00	0	0.00	0.00
Sum:	93.06	106.62	97.50	102.31	99.73	103.37	96.70	112.79	94.28	90.76	102.87	0.00		2376248	100	61508923	100	1538
NC:	11													**% Map**				
Avg TPR:	0.861													3.86				
Acc:	0.886																	

Confusion Matrix (Pixels*) *Subject to round-off error associated with calculating pixels from % reference class with 2 decimal places

	Predicted																			
Reference	**1**	**2**	**3**	**4**	**5**	**6**	**7**	**8**	**9**	**10**	**11**	**12**	**Support**	**N**	**TP**	**FN**	**TPR**	**PPV**	**FNR**	**F1**
1	49938	3753	0	0	0	0	0	0	0	0	0	0	53691	2322500	49938	3753	0.930	0.990	0.070	0.959
2	515	1025897	0	2368	0	103	0	103	0	0	618	0	1029604	1346587	1025897	3707	0.996	0.996	0.004	0.996
3	0	0	37172	921	0	269	0	0	4	0	0	0	38365	2337826	37172	1193	0.969	0.975	0.031	0.972
4	0	0	6	10079	3	0	34	0	0	9	4	0	10136	2366055	10079	57	0.994	0.738	0.006	0.847
5	0	0	0	102	87037	0	8763	18766	13	1254	11986	0	127920	2248271	87037	40883	0.680	0.687	0.320	0.684
6	0	0	866	0	0	148558	0	0	10756	3269	0	0	163450	2212741	148558	14892	0.909	0.760	0.091	0.828
7	0	0	0	0	3107	0	28235	1670	3	192	1013	0	34220	2341971	28235	5985	0.825	0.552	0.175	0.662
8	0	0	0	8	3209	0	1219	35201	50	37	1889	0	41614	2334577	35201	6413	0.846	0.513	0.154	0.639
9	0	0	79	0	3679	45298	2769	396	321401	21917	158	0	395698	1980493	321401	74297	0.812	0.910	0.188	0.858
10	0	0	0	0	17658	1143	9071	1523	20428	259810	36596	0	346229	2029962	259810	86419	0.750	0.880	0.250	0.810
11	0	0	0	176	11959	0	1015	10971	555	8739	101851	0	135264	2240927	101851	33414	0.753	0.661	0.247	0.704
12	0	0	0	0	0	0	0	0	0	0	0	0	0	2376191	0	0				
Sum:	50453	1029650	38123	13655	126651	195370	51106	68629	353209	295228	154116	0	2376191							
FP:	515	3753	952	3576	39614	46812	22872	33429	31808	35417	52265	0				**Avg:**	0.861	0.788	0.139	0.814
TN:	2321985	1342834	2336875	2362480	2208657	2165929	2319100	2301148	1948685	1994545	2188662	2376191				**Acc:**	0.886			

A3. RI05 MS+TPI confusion matrix, prevalence, and performance metrics.

Study Site RI05
MS+T+TPI

Confusion Matrix (% Reference Class)

	Predicted																	
Reference	**1**	**2**	**3**	**4**	**5**	**6**	**7**	**8**	**9**	**10**	**11**	**12**	**Sum**	**Reference Pixels**	**Prevalence % Reference**	**Predicted Pixels**	**Prevalence % Map**	**Predicted Area (ha)**
1	88.65	11.35	0.00	0.00	0.00	0.00	0.00	0.00	0.00	0.00	0.00		100.0	53691	2.26	74474	0.12	1.86
2	0.00	99.77	0.00	0.12	0.00	0.00	0.03	0.01	0.00	0.00	0.07		100.0	1029707	43.33	10119274	16.45	252.98
3	0.00	0.00	98.87	0.48	0.00	0.63	0.00	0.00	0.01	0.00	0.00		100.0	38365	1.61	700490	1.14	17.51
4	0.00	0.00	0.04	99.50	0.03	0.00	0.28	0.00	0.00	0.08	0.08		100.0	10135	0.43	554153	0.90	13.85
5	0.00	0.00	0.00	0.09	76.21	0.00	5.86	12.82	0.00	1.28	3.75		100.0	127920	5.38	2776456	4.51	69.41
6	0.00	0.00	0.39	0.00	0.00	94.42	0.00	0.00	5.19	0.00	0.00		100.0	163466	6.88	4019194	6.53	100.48
7	0.00	0.00	0.00	0.00	7.21	0.00	86.03	2.46	0.00	1.70	2.60		100.0	34220	1.44	3248550	5.28	81.21
8	0.00	0.00	0.00	0.00	6.46	0.00	1.42	90.98	0.00	0.19	0.95		100.0	41618	1.75	1306060	2.12	32.65
9	0.00	0.00	0.02	0.00	0.00	8.55	0.00	0.00	88.30	3.12	0.00		100.0	395619	16.65	15561078	25.30	389.03
10	0.00	0.00	0.00	0.00	2.36	0.04	3.14	0.00	2.57	81.36	10.53		100.0	346229	14.57	13451145	21.87	336.28
11	0.00	0.00	0.00	0.12	3.44	0.02	0.62	0.40	0.75	6.76	87.89		100.0	135278	5.69	9698049	15.77	242.45
12													0.0	0	0.00	0	0.00	0.00
Sum:	88.7	111.1	99.3	100.3	95.7	103.7	97.4	106.7	96.8	94.5	105.9	0.0		2376248	100	61508923	100	1538
NC:	11													**% Map**				
Avg TPR:	0.902													3.86				
Acc:	0.922																	

Confusion Matrix (Pixels*) *Subject to round-off error associated with calculating pixels from % reference class with 2 decimal places

	Predicted																			
Reference	**1**	**2**	**3**	**4**	**5**	**6**	**7**	**8**	**9**	**10**	**11**	**12**	**Support**	**N**	**TP**	**FN**	**TPR**	**PPV**	**FNR**	**F1**
1	47597	6094	0	0	0	0	0	0	0	0	0	0	53691	2322527	47597	6094	0.887	1.000	0.114	0.940
2	0	1027339	0	1236	0	0	309	103	0	0	721	0	1029707	1346511	1027339	2368	0.998	0.994	0.002	0.996
3	0	0	37931	184	0	242	0	0	4	0	0	0	38361	2337857	37931	430	0.989	0.981	0.011	0.985
4	0	0	4	10084	3	0	28	0	0	8	8	0	10136	2366082	10084	52	0.995	0.856	0.005	0.920
5	0	0	0	115	97488	0	7496	16399	0	1637	4797	0	127933	2248286	97488	30445	0.762	0.844	0.238	0.801
6	0	0	638	0	0	154345	0	0	8484	0	0	0	163466	2212752	154345	9121	0.944	0.818	0.056	0.877
7	0	0	0	0	2467	0	29439	842	0	582	890	0	34220	2341998	29439	4781	0.860	0.594	0.140	0.703
8	0	0	0	0	2689	0	591	37864	0	79	395	0	41618	2334600	37864	3754	0.910	0.679	0.090	0.778
9	0	0	79	0	0	33825	0	0	349332	12343	0	0	395579	1980639	349332	46248	0.883	0.950	0.117	0.915
10	0	0	0	0	8171	138	10872	0	8898	281692	36458	0	346229	2029989	281692	64537	0.814	0.922	0.186	0.864
11	0	0	0	162	4654	27	839	541	1015	9145	118896	0	135278	2240940	118896	16382	0.879	0.733	0.121	0.799
12	0	0	0	0	0	0	0	0	0	0	0	0	0	2376218	0	0				
Sum:	47597	1033433	38652	11782	115471	188577	49574	55749	367732	305486	162165	0	2376218							
FP:	0	6094	721	1697	17983	34233	20135	17885	18400	23794	43269	0				**Avg:**	0.902	0.852	0.098	0.871
TN:	2322527	1340417	2337137	2364385	2230302	2178520	2321864	2316715	1962239	2006195	2197671	2376218				**Acc:**	0.922			

Confusion Matrix (% Population Area)** **Prevalence-weighted

	Predicted														
Reference	**1**	**2**	**3**	**4**	**5**	**6**	**7**	**8**	**9**	**10**	**11**	**12**	**Sum**	**TP**	**TPR**
1	0.121	0.097	0.000	0.000	0.000	0.000	0.000	0.000	0.000	0.000	0.000		0.218	0.121	0.555
2	0.000	16.355	0.000	0.094	0.000	0.000	0.033	0.004	0.000	0.000	0.070		16.556	16.355	0.988
3	0.000	0.000	1.118	0.014	0.000	0.008	0.000	0.000	0.000	0.000	0.000		1.140	1.118	0.980
4	0.000	0.000	0.000	0.771	0.000	0.000	0.003	0.000	0.000	0.001	0.001		0.776	0.771	0.994
5	0.000	0.000	0.000	0.009	3.811	0.000	0.799	0.625	0.000	0.117	0.466		5.827	3.811	0.654
6	0.000	0.000	0.019	0.000	0.000	5.348	0.000	0.000	0.584	0.000	0.000		5.951	5.348	0.899
7	0.000	0.000	0.000	0.000	0.096	0.000	3.136	0.032	0.000	0.042	0.087		3.393	3.136	0.924
8	0.000	0.000	0.000	0.000	0.105	0.000	0.063	1.442	0.000	0.006	0.038		1.654	1.442	0.872
9	0.000	0.000	0.002	0.000	0.000	1.172	0.000	0.000	24.033	0.884	0.000		26.091	24.033	0.921
10	0.000	0.000	0.000	0.000	0.319	0.005	1.158	0.000	0.612	20.165	3.545		25.805	20.165	0.781
11	0.000	0.000	0.000	0.012	0.182	0.001	0.089	0.021	0.070	0.655	11.560		12.590	11.560	0.918
12													0.000	0.000	
Sum:	0.12	16.45	1.14	0.90	4.51	6.53	5.28	2.12	25.30	21.87	15.77	0.00	100.00		
PPV:	1.000	0.994	0.981	0.856	0.844	0.818	0.594	0.679	0.950	0.922	0.733			**Avg:**	0.862
														Acc:	0.879

A4. RI05 MS+T+TPI confusion matrix, prevalence, and performance metrics including population proportional area.

APPENDIX B

Study Site RI08
MS

Confusion Matrix (% Reference Class)

	Predicted																	
Reference	**1**	**2**	**3**	**4**	**5**	**6**	**7**	**8**	**9**	**10**	**11**	**12**	**Sum**	**Reference Pixels**	**Prevalence % Reference**	**Predicted Pixels**	**Prevalence % Map**	**Predicted Area (ha)**
1	99.17	0.81	0.00	0.00	0.00	0.00	0.00	0.00	0.00	0.00	0.00	0.02	100.0	699406	34.01	2039427	6.58	50.99
2	0.22	98.62	0.00	0.83	0.03	0.09	0.00	0.20	0.00	0.00	0.00	0.01	100.0	799733	38.89	6761911	21.83	169.05
3	0.00	0.00	98.59	0.14	0.00	1.26	0.00	0.00	0.01	0.01	0.00	0.00	100.0	17179	0.84	570684	1.84	14.27
4	0.00	0.00	0.62	98.24	0.03	0.97	0.01	0.00	0.00	0.00	0.12	0.00	100.0	9851	0.48	468780	1.51	11.72
5	0.00	0.00	0.00	0.00	67.74	0.15	12.91	8.72	2.33	0.73	7.41	0.00	100.0	113848	5.54	3143785	10.15	78.59
6	0.00	0.00	0.05	0.87	0.43	80.12	0.51	5.50	3.48	1.57	0.16	7.32	100.0	29545	1.44	1371563	4.43	34.29
7	0.00	0.00	0.00	0.00	14.19	0.01	53.05	3.40	6.90	17.48	4.97	0.00	100.0	6786	0.33	2615625	8.44	65.39
8	0.00	0.00	0.00	0.00	6.42	1.78	1.39	81.98	4.11	2.32	2.00	0.00	100.0	50893	2.47	2681126	8.66	67.03
9	0.00	0.00	0.00	0.00	9.06	4.35	14.49	15.21	42.36	13.27	0.91	0.35	100.0	176061	8.56	3583739	11.57	89.59
10	0.00	0.00	0.00	0.00	1.64	1.77	3.99	5.34	12.11	65.56	9.58	0.00	100.0	99537	4.84	4912826	15.86	122.82
11	0.00	0.00	0.00	0.00	2.01	0.18	1.24	1.43	0.16	11.24	83.73	0.00	100.0	47350	2.30	2641528	8.53	66.04
12	0.00	0.00	0.03	0.00	0.00	5.80	0.03	0.07	0.24	0.41	0.00	93.42	100.0	6139	0.30	185951	0.60	4.65
Sum:	99.39	99.43	99.29	100.08	101.55	96.48	87.62	121.85	71.70	112.59	108.88	101.12		2056328	100	30976945	100	774
NC:	12													**% Map**				
Avg TPR:	0.802													6.64				
Acc:	0.895																	

Confusion Matrix (Pixels*)   *Subject to round-off error associated with calculating pixels from % reference class with 2 decimal places

	Predicted																			
Reference	**1**	**2**	**3**	**4**	**5**	**6**	**7**	**8**	**9**	**10**	**11**	**12**	**Support**	**N**	**TP**	**FN**	**TPR**	**PPV**	**FNR**	**F1**
1	693601	5665	0	0	0	0	0	0	0	0	0	140	699406	1356900	693601	5805	0.992	0.997	0.008	0.995
2	1759	788697	0	6638	240	720	0	1599	0	0	0	80	799733	1256573	788697	11036	0.986	0.993	0.014	0.990
3	0	0	16937	24	0	216	0	0	2	2	0	0	17181	2039125	16937	244	0.986	0.995	0.014	0.991
4	0	0	61	9678	3	96	1	0	0	0	12	0	9850	2046456	9678	172	0.982	0.583	0.018	0.732
5	0	0	0	0	77121	171	14698	9928	2653	831	8436	0	113837	1942469	77121	36716	0.677	0.769	0.323	0.720
6	0	0	15	257	127	23671	151	1625	1028	464	47	2163	29548	2026758	23671	5877	0.801	0.664	0.199	0.726
7	0	0	0	0	963	1	3600	231	468	1186	337	0	6786	2049520	3600	3186	0.531	0.073	0.470	0.129
8	0	0	0	0	3267	906	707	41722	2092	1181	1018	0	50893	2005413	41722	9171	0.820	0.475	0.180	0.601
9	0	0	0	0	15951	7659	25511	26779	74579	23363	1602	616	176061	1880245	74579	101482	0.424	0.802	0.576	0.554
10	0	0	0	0	1632	1762	3972	5315	12054	65256	9536	0	99527	1956779	65256	34271	0.656	0.668	0.344	0.662
11	0	0	0	0	952	85	587	677	76	5322	39646	0	47345	2008960	39646	7699	0.837	0.654	0.163	0.734
12	0	0	2	0	0	356	2	4	15	25	0	5735	6139	2050167	5735	404	0.934	0.657	0.066	0.771
Sum:	695360	794362	17014	16596	100256	35642	49229	87880	92966	97631	60634	8734	2056306							
FP:	1759	5665	78	6919	23135	11971	45629	46158	18387	32374	20988	2999				**Avg:**	0.802	0.694	0.198	0.717
TN:	1355140	1250907	2039047	2039537	1919334	2014787	2003891	1959254	1861858	1924404	1987972	2047168				**Acc:**	0.895			

N	Negatives	Number of negatives for class
TP	True Positive	Number of pixels correctly predicted as x for class x
FN	False Negative	Number of pixels incorrectly predicted as not x for class x
FP	False Positive	Number of pixels incorrectly predicted as x for not class x
TN	True Negative	Number of pixels correctly predicted as not x for not class x
TPR	True Positive Rate (Producer's Accuracy or Recall)	How often is x predicted for class x (conditional probability of correct prediction)
PPV	Positive Predictive Value (User's Accuracy, or Precision)	How often the prediction of x is correct (posterior probability of correct prediction)
FNR	False Negative Rate	How often not x is predicted for class x
Acc	Accuracy	How often the classification is correct
F1	F1 Score	Harmonic mean of TPR and PPV

B1. RI08 MS confusion matrix, prevalence, and performance metrics.

Study Site RI08
MS+T

Confusion Matrix (% Reference Class)

Reference	Predicted 1	2	3	4	5	6	7	8	9	10	11	12	Sum	Reference Pixels	Prevalence % Reference	Predicted Pixels	Prevalence % Map	Predicted Area (ha)
1	98.78	1.16	0.00	0.03	0.00	0.00	0.00	0.00	0.00	0.00	0.00	0.03	100.0	699406	34.01	1944423	6.28	48.61
2	0.16	98.99	0.00	0.51	0.23	0.01	0.00	0.05	0.04	0.00	0.00	0.00	100.0	799733	38.89	6595761	21.29	164.89
3	0.00	0.00	98.84	0.28	0.00	0.86	0.00	0.00	0.02	0.00	0.00	0.00	100.0	17179	0.84	393076	1.27	9.83
4	0.00	0.00	0.48	98.41	0.10	0.96	0.05	0.00	0.00	0.00	0.00	0.00	100.0	9851	0.48	626717	2.02	15.67
5	0.00	0.00	0.00	0.00	81.26	0.26	6.62	2.75	4.87	1.73	2.50	0.00	100.0	113848	5.54	3805988	12.29	95.15
6	0.00	0.00	0.05	0.74	0.01	81.31	0.00	0.00	11.86	0.14	0.00	5.88	100.0	29545	1.44	2094144	6.76	52.35
7	0.00	0.00	0.00	0.00	7.53	0.01	74.83	3.04	0.31	13.26	1.02	0.00	100.0	6786	0.33	1686165	5.44	42.15
8	0.00	0.00	0.00	0.00	5.40	0.53	3.77	86.26	0.23	2.61	1.21	0.00	100.0	50893	2.47	1242203	4.01	31.06
9	0.00	0.00	0.00	0.00	4.01	3.19	1.28	0.00	85.43	5.68	0.10	0.31	100.0	176061	8.56	7363428	23.77	184.09
10	0.00	0.00	0.00	0.00	2.34	1.25	5.69	6.70	4.55	70.85	8.63	0.00	100.0	99537	4.84	3653506	11.79	91.34
11	0.00	0.00	0.00	0.00	1.75	0.07	2.23	1.68	0.00	8.68	85.59	0.00	100.0	47350	2.30	1354225	4.37	33.86
12	0.00	0.00	0.03	0.00	0.00	5.64	0.00	0.00	0.23	0.00	0.00	94.10	100.0	6139	0.30	217309	0.70	5.43
SUM:	98.94	100.15	99.40	99.97	102.63	94.09	94.47	100.48	107.54	102.95	99.05	100.32		2056328	100	30976945	100	774
NC:	12													% Map				
Avg TPR:	0.879													6.64				
Acc:	0.944																	

Confusion Matrix (Pixels*) *Subject to round-off error associated with calculating pixels from % reference class with 2 decimal places

Reference	Predicted 1	2	3	4	5	6	7	8	9	10	11	12	Support	N	TP	FN	TPR	PPV	FNR	F1
1	690873	8113	0	210	0	0	0	0	0	0	0	210	699406	1356843	690873	8533	0.988	0.998	0.012	0.993
2	1280	791656	0	4079	1839	80	0	400	320	0	0	0	799653	1256596	791656	7997	0.990	0.990	0.010	0.990
3	0	0	16980	48	0	148	0	0	3	0	0	0	17179	2039070	16980	199	0.988	0.996	0.012	0.992
4	0	0	47	9694	10	95	5	0	0	0	0	0	9851	2046398	9694	157	0.984	0.680	0.016	0.804
5	0	0	0	0	92513	296	7537	3131	5544	1970	2846	0	113837	1942412	92513	21324	0.813	0.858	0.187	0.835
6	0	0	15	219	3	24023	0	0	3504	41	0	1737	29542	2026707	24023	5519	0.813	0.747	0.187	0.779
7	0	0	0	0	511	1	5078	206	21	900	69	0	6786	2049463	5078	1708	0.748	0.216	0.252	0.335
8	0	0	0	0	2748	270	1919	43900	117	1328	616	0	50898	2005351	43900	6998	0.863	0.797	0.137	0.828
9	0	0	0	0	7060	5616	2254	0	150409	10000	176	546	176061	1880188	150409	25652	0.854	0.915	0.146	0.883
10	0	0	0	0	2329	1244	5664	6669	4529	70522	8590	0	99547	1956702	70522	29025	0.708	0.794	0.292	0.749
11	0	0	0	0	829	33	1056	795	0	4110	40527	0	47350	2008899	40527	6823	0.856	0.767	0.144	0.809
12	0	0	2	0	0	346	0	0	14	0	0	5777	6139	2050110	5777	362	0.941	0.699	0.059	0.802
Sum:	692153	799769	17044	14250	107842	32152	23511	55102	164462	88871	52824	8270	2056249							
FP:	1280	8113	64	4555	15329	8129	18433	11201	14053	18349	12297	2493				Avg:	0.879	0.788	0.121	0.817
TN:	1355563	1248483	2039006	2041843	1927083	2018578	2031029	1994149	1866135	1938352	1996601	2047617				Acc:	0.944			

B2. RI08 MS+T confusion matrix, prevalence, and performance metrics.

Study Site RI08
MS+TPI

Confusion Matrix (% Reference Class)

	Predicted																	
Reference	**1**	**2**	**3**	**4**	**5**	**6**	**7**	**8**	**9**	**10**	**11**	**12**	**Sum**	**Reference Pixels**	**Prevalence % Reference**	**Predicted Pixels**	**Prevalence % Map**	**Predicted Area (ha)**
1	99.01	0.34	0.00	0.00	0.00	0.00	0.00	0.00	0.00	0.00	0.00	0.65	100.0	699406	34.01	2088410	6.74	52.21
2	0.18	98.85	0.00	0.67	0.01	0.00	0.00	0.28	0.00	0.00	0.00	0.01	100.0	799733	38.89	6524148	21.06	163.10
3	0.00	0.00	98.67	0.24	0.00	1.08	0.00	0.00	0.01	0.00	0.00	0.00	100.0	17179	0.84	700493	2.26	17.51
4	0.00	0.00	0.65	98.27	0.00	0.88	0.00	0.02	0.00	0.00	0.17	0.00	100.0	9851	0.48	349285	1.13	8.73
5	0.00	0.00	0.00	0.00	90.70	0.01	3.64	0.67	0.00	0.01	4.97	0.00	100.0	113848	5.54	1367489	4.41	34.19
6	0.00	0.00	0.05	0.10	0.00	85.54	0.00	0.00	3.38	4.65	0.00	6.27	100.0	29545	1.44	1898537	6.13	47.46
7	0.00	0.00	0.00	0.00	6.10	0.06	83.85	2.23	0.00	0.97	6.79	0.00	100.0	6786	0.33	4044934	13.06	101.12
8	0.00	0.00	0.00	0.00	2.68	0.10	4.04	90.80	0.00	0.00	2.37	0.00	100.0	50893	2.47	1359771	4.39	33.99
9	0.00	0.00	0.00	0.00	0.00	3.56	0.00	0.00	91.69	4.49	0.01	0.26	100.0	176061	8.56	3063086	9.89	76.58
10	0.00	0.00	0.00	0.00	0.00	2.12	0.38	0.00	3.37	93.50	0.62	0.01	100.0	99537	4.84	6300102	20.34	157.50
11	0.00	0.00	0.00	0.00	0.27	0.13	4.57	1.86	0.00	1.89	91.28	0.00	100.0	47350	2.30	2837767	9.16	70.94
12	0.00	0.00	0.03	0.00	0.00	5.36	0.00	0.00	0.42	0.37	0.00	93.81	100.0	6139	0.30	442923	1.43	11.07
Sum:	99.19	99.19	99.40	99.28	99.76	98.84	96.48	95.86	98.87	105.88	106.21	101.01		2056328	100	30976945	100	774
NC:	12													**% Map**				
Avg TPR:	0.930													6.64				
Acc:	0.969																	

Confusion Matrix (Pixels*) *Subject to round-off error associated with calculating pixels from % reference class with 2 decimal places

	Predicted																				
Reference	**1**	**2**	**3**	**4**	**5**	**6**	**7**	**8**	**9**	**10**	**11**	**12**	**Support**	**N**	**TP**	**FN**	**TPR**	**PPV**	**FNR**	**F1**
1	692482	2378	0	0	0	0	0	0	0	0	0	4546	699406	1356930	692482	6924	0.990	0.998	0.010	0.994
2	1440	790536	0	5358	80	0	0	2239	0	0	0	80	799733	1256603	790536	9197	0.989	0.997	0.012	0.993
3	0	0	16951	41	0	186	0	0	2	0	0	0	17179	2039157	16951	228	0.987	0.995	0.013	0.991
4	0	0	64	9681	0	87	0	2	0	0	17	0	9850	2046486	9681	169	0.983	0.641	0.017	0.776
5	0	0	0	0	103260	11	4144	763	0	11	5658	0	113848	1942488	103260	10588	0.907	0.981	0.093	0.943
6	0	0	15	30	0	25273	0	0	999	1374	0	1852	29542	2026794	25273	4269	0.855	0.735	0.145	0.791
7	0	0	0	0	414	4	5690	151	0	66	461	0	6786	2049550	5690	1096	0.839	0.394	0.162	0.536
8	0	0	0	0	1364	51	2056	46211	0	0	1206	0	50888	2005448	46211	4677	0.908	0.920	0.092	0.914
9	0	0	0	0	0	6268	0	0	161430	7905	18	458	176079	1880257	161430	14648	0.917	0.974	0.083	0.944
10	0	0	0	0	0	2110	378	0	3354	93067	617	10	99537	1956799	93067	6470	0.935	0.901	0.065	0.917
11	0	0	0	0	128	62	2164	881	0	895	43221	0	47350	2008986	43221	4129	0.913	0.844	0.087	0.877
12	0	0	2	0	0	329	0	0	26	23	0	5759	6138	2050198	5759	379	0.938	0.453	0.062	0.611
Sum:	693921	792914	17031	15110	105246	34380	14432	50247	165811	103341	51198	12705	2056336							
FP:	1440	2378	81	5429	1986	9107	8742	4036	4381	10274	7977	6946				**Avg:**	0.930	0.819	0.070	0.857
TN:	1355490	1254225	2039076	2041057	1940502	2017687	2040808	2001412	1875877	1946525	2001009	2043251				**Acc:**	0.969			

B3. RI08 MS+TPI confusion matrix, prevalence, and performance metrics.

Study Site RI08
MS+T+TPI

Confusion Matrix (% Reference Class)

	Predicted																	
Reference	1	2	3	4	5	6	7	8	9	10	11	12	Sum	Reference Pixels	Prevalence % Reference	Predicted Pixels	Prevalence % Map	Predicted Area (ha)
1	98.91	0.44	0.00	0.00	0.00	0.00	0.00	0.00	0.00	0.00	0.00	0.64	100.0	699406	34.01	1983250	6.40	49.58
2	0.16	98.98	0.00	0.57	0.01	0.01	0.00	0.26	0.00	0.00	0.00	0.00	100.0	799733	38.89	6553229	21.16	163.83
3	0.00	0.00	98.97	0.35	0.00	0.61	0.00	0.00	0.05	0.00	0.00	0.02	100.0	17179	0.84	485570	1.57	12.14
4	0.00	0.00	0.45	98.62	0.00	0.84	0.08	0.00	0.00	0.00	0.01	0.00	100.0	9851	0.48	423843	1.37	10.60
5	0.00	0.00	0.00	0.00	95.79	0.49	1.85	0.30	0.00	0.00	1.57	0.00	100.0	113848	5.54	1976333	6.38	49.41
6	0.00	0.00	0.09	0.16	0.00	90.08	0.00	0.00	4.29	0.75	0.00	4.62	100.0	29545	1.44	4648474	15.01	116.21
7	0.00	0.00	0.00	0.00	2.36	0.04	92.54	2.42	0.00	0.07	2.56	0.00	100.0	6786	0.33	2338214	7.55	58.46
8	0.00	0.00	0.00	0.00	1.91	0.00	4.42	92.37	0.00	0.00	1.30	0.00	100.0	50893	2.47	1228060	3.96	30.70
9	0.00	0.00	0.00	0.00	0.00	2.35	0.00	0.00	92.84	4.57	0.01	0.23	100.0	176061	8.56	2841250	9.17	71.03
10	0.00	0.00	0.00	0.00	0.00	1.60	0.04	0.00	3.04	94.82	0.50	0.00	100.0	99537	4.84	5979578	19.30	149.49
11	0.00	0.00	0.00	0.00	0.06	0.03	1.86	1.85	0.00	1.63	94.56	0.00	100.0	47350	2.30	2014497	6.50	50.36
12	0.00	0.00	0.03	0.00	0.00	5.49	0.00	0.00	0.11	0.00	0.00	94.36	100.0	6139	0.30	504647	1.63	12.62
Sum:	99.07	99.42	99.54	99.70	100.13	101.54	100.79	97.20	100.33	101.84	100.51	99.87		2056328	100	30976945	100	774
NC:	12													% Map				
Avg TPR:	0.952													6.64				
Acc:	0.976																	

Confusion Matrix (Pixels*) *Subject to round-off error associated with calculating pixels from % reference class with 2 decimal places

	Predicted																				
Reference	1	2	3	4	5	6	7	8	9	10	11	12	Support	N	TP	FN	TPR	PPV	FNR	F1
1	691782	3077	0	0	0	0	0	0	0	0	0	4476	699336	1356833	691782	7554	0.989	0.998	0.011	0.994
2	1280	791576	0	4558	80	80	0	2079	0	0	0	0	799653	1256516	791576	8077	0.990	0.996	0.010	0.993
3	0	0	17002	60	0	105	0	0	9	0	0	3	17179	2038990	17002	177	0.990	0.996	0.010	0.993
4	0	0	44	9715	0	83	8	0	0	0	1	0	9851	2046318	9715	136	0.986	0.676	0.014	0.802
5	0	0	0	0	109055	558	2106	342	0	0	1787	0	113848	1942321	109055	4793	0.958	0.989	0.042	0.973
6	0	0	27	47	0	26614	0	0	1267	222	0	1365	29542	2026627	26614	2928	0.901	0.794	0.099	0.844
7	0	0	0	0	160	3	6280	164	0	5	174	0	6785	2049384	6280	506	0.925	0.543	0.075	0.684
8	0	0	0	0	972	0	2249	47010	0	0	662	0	50893	2005276	47010	3883	0.924	0.931	0.076	0.928
9	0	0	0	0	0	4137	0	0	163455	8046	18	405	176061	1880108	163455	12606	0.928	0.974	0.072	0.951
10	0	0	0	0	0	1593	40	0	3026	94381	498	0	99537	1956632	94381	5156	0.948	0.913	0.052	0.930
11	0	0	0	0	28	14	881	876	0	772	44774	0	47345	2008824	44774	2571	0.946	0.934	0.054	0.940
12	0	0	2	0	0	337	0	0	7	0	0	5793	6138	2050031	5793	346	0.944	0.481	0.056	0.637
Sum:	693062	794653	17075	14381	110296	33523	11564	50471	167764	103425	47913	12042	2056169							
FP:	1280	3077	73	4666	1241	6909	5284	3461	4309	9044	3139	6250				Avg:	0.952	0.852	0.048	0.889
TN:	1355553	1253439	2038917	2041652	1941081	2019718	2044100	2001815	1875799	1947588	2005685	2043781				Acc:	0.976			

Confusion Matrix (% Population Area)** **Prevalence-weighted

	Predicted														
Reference	1	2	3	4	5	6	7	8	9	10	11	12	Sum	TP	TPR
1	6.391	0.082	0.000	0.000	0.000	0.000	0.000	0.000	0.000	0.000	0.000	0.606	7.078	6.391	0.903
2	0.012	21.073	0.000	0.434	0.005	0.036	0.000	0.163	0.000	0.000	0.000	0.000	21.723	21.073	0.970
3	0.000	0.000	1.561	0.006	0.000	0.047	0.000	0.000	0.000	0.000	0.000	0.000	1.614	1.561	0.967
4	0.000	0.000	0.004	0.924	0.000	0.037	0.005	0.000	0.000	0.000	0.000	0.000	0.971	0.924	0.952
5	0.000	0.000	0.000	0.000	6.308	0.250	1.375	0.027	0.000	0.000	0.243	0.000	8.202	6.308	0.769
6	0.000	0.000	0.002	0.004	0.000	11.913	0.000	0.000	0.069	0.041	0.000	0.185	12.216	11.913	0.975
7	0.000	0.000	0.000	0.000	0.009	0.001	4.099	0.013	0.000	0.001	0.024	0.000	4.147	4.099	0.988
8	0.000	0.000	0.000	0.000	0.056	0.000	1.468	3.693	0.000	0.000	0.090	0.000	5.307	3.693	0.696
9	0.000	0.000	0.000	0.000	0.000	1.852	0.000	0.000	8.937	1.502	0.002	0.055	12.348	8.937	0.724
10	0.000	0.000	0.000	0.000	0.000	0.713	0.026	0.000	0.165	17.615	0.068	0.000	18.587	17.615	0.948
11	0.000	0.000	0.000	0.000	0.002	0.006	0.575	0.069	0.000	0.144	6.077	0.000	6.873	6.077	0.884
12	0.000	0.000	0.000	0.000	0.000	0.151	0.000	0.000	0.000	0.000	0.000	0.784	0.935	0.784	0.838
SUM:	6.40	21.16	1.57	1.37	6.38	15.01	7.55	3.96	9.17	19.30	6.50	1.63	100.00		
PPV	0.998	0.996	0.996	0.676	0.989	0.794	0.543	0.931	0.974	0.913	0.934	0.481		Avg:	0.885
														Acc:	0.894

B4. RI08 MS+T+TPI confusion matrix, prevalence, and performance metrics including population proportional area.